Review

Jiang Li, Chaoyue Liu, Haitao Chen, Jingshu Guo, Ming Zhang and Daoxin Dai*

Hybrid silicon photonic devices with two-dimensional materials

Abstract: Silicon photonics is becoming more and more attractive in the applications of optical interconnections, optical computing, and optical sensing. Although various silicon photonic devices have been developed rapidly, it is still not easy to realize active photonic devices and circuits with silicon alone due to the intrinsic limitations of silicon. In recent years, two-dimensional (2D) materials have attracted extensive attentions due to their unique properties in electronics and photonics. 2D materials can be easily transferred onto silicon and thus provide a promising approach for realizing active photonic devices on silicon. In this paper, we give a review on recent progresses towards hybrid silicon photonics devices with 2D materials, including two parts. One is silicon-based photodetectors with 2D materials for the wavelength-bands from ultraviolet (UV) to mid-infrared (MIR). The other is silicon photonic switches/modulators with 2D materials, including high-speed electro-optical modulators, high-efficiency thermal-optical switches and low-threshold all-optical modulators, etc. These hybrid silicon photonic devices with 2D materials devices provide an alternative way for the realization of multifunctional silicon photonic integrated circuits in the future.

*Corresponding author: Daoxin Dai, State Key Laboratory for Modern Optical Instrumentation, College of Optical Science and Engineering, International Research Center for Advanced Photonics, Zijingang Campus, Zhejiang University, Hangzhou, China; and Ningbo Research Institute, Zhejiang University, Ningbo 315100, China, E-mail: dxdai@zju.edu.cn. https://orcid.org/0000-0002-2769-3009
Jiang Li, Chaoyue Liu, Haitao Chen and Jingshu Guo: State Key Laboratory for Modern Optical Instrumentation, College of Optical Science and Engineering, International Research Center for Advanced Photonics, Zijingang Campus, Zhejiang University, Hangzhou, China. https://orcid.org/0000-0002-0272-2264 (H. Chen). https://orcid.org/0000-0003-3623-6990 (J. Guo)
Ming Zhang: State Key Laboratory for Modern Optical Instrumentation, College of Optical Science and Engineering, International Research Center for Advanced Photonics, Zijingang Campus, Zhejiang University, Hangzhou, China; Ningbo Research Institute, Zhejiang University, Ningbo 315100, China

1 Introduction

In the past decades, silicon photonics has become very popular for many applications because of the unique advantages of CMOS compatibility and high integrated density [1–4]. As it is well known, high-performance passive silicon photonic devices with compact footprints have been realized for optical interconnects and optical sensing, such as multi-channel optical filters [5, 6], polarization-handling devices [7, 8], and multimode photonic devices [9, 10]. In contrast, it is usually very challenging to realize active photonic devices with pure silicon due to the intrinsic material properties of silicon, although great efforts have been made in the past years. In order to compensate the drawbacks of silicon, currently silicon-plus photonics has attracted intensive attention as a promising solution by introducing some other optoelectronic materials [11, 12]. For example, people have tried to introduce various functional materials to work together with silicon, including metals [13], III–V semiconductors [14, 15], germanium [16], two-dimensional (2D) materials [17–20], polymer [21, 22], magnetic-optical materials [23], and liquid-crystals [24].

As demonstrated previously, traditional semiconductor materials have been introduced to realize active photonic devices on silicon successfully, such as lasers [25–27], photodetectors [28, 29], and modulators [30, 31]. In this case, one of the most troublesome issues is the compatibility of the introduced materials in the fabrication processes as well as the structural design. When traditional semiconductor materials are introduced, special processes are usually needed due to the thermal expansion and lattice mismatch [32]. For example, some special germanium-growth process is required for the fabrication of high-speed silicon/germanium photodetectors and modulators [33, 34], while special bonding technologies were introduced for realizing hybrid silicon/III–V lasers, modulators and photodetectors [35]. These hybrid active silicon photonic

devices have been used successfully for the applications of optical fiber communications operating with the near-infrared (near-IR) wavelength-band of 1.31/1.55 μm [12, 36].

More recently it is also very interesting to develop silicon photonics beyond 1.31/1.55 μm for many important applications in optical communication [37], nonlinear photonics [38], lidar [39], and optical bio-sensing [40]. For example, for some bio-molecules and gases such as glucose, CH_4, CO_2, and CO, there are strong overtone and combination absorption lines in the wavelength range of 2–3 μm [41]. However, those popular semiconductor materials (such as Ge, InP, etc.) become unavailable regarding that their cut-off wavelength for light absorption is limited by the bandgap and cannot be modified freely. As an alternative, 2D materials have attracted intensive attention owning to their unique properties, such as ultra-high carrier mobility and strong light absorption in a broad wavelength-band [42–49], which makes them promising for developing photonic devices for the wavelength-bands beyond 1.3/1.55 μm [50, 51]. For example, currently graphene has been used widely as a well-known 2D material because of the extremely broad absorption wavelength-band ranging from ultraviolet (UV) to far-infrared (FIR) [42, 52, 53]. Furthermore, graphene has ultra-high carrier mobility (up to ~200,000 $cm^2 V^{-1} s^{-1}$), tunable Fermi level as well as high thermal conductivity [43]. For mono-layer graphene, there is ~2.3% absorption for normal illuminated light [44, 54], which is strong regarding the atom-level thickness. On the other hand, it is very desired to further enhance the light–matter interaction when using 2D materials, which is important for achieving high responsivity photodetectors, high-speed modulators, and low-threshold all-optical devices. Currently some graphene photodetectors have been demonstrated with strong absorption and enhanced responsivities for short-wave photodetection by introducing some wide-bandgap quantum dots [55–58], nanoparticles [59–61], or nanostructures [62]. In addition, optical micro-cavities have also often been used for enhancing the light–matter interaction with 2D materials [63, 64].

Another promising approach is combining 2D materials and photonic waveguides, in which way the light–matter interaction length can be extended very effectively. Currently, high-speed hybrid silicon/2D material waveguide photodetectors and modulators have been demonstrated for 1.3/1.55 μm as well as 2 μm and beyond [45, 46]. Furthermore, some 2D materials are very transparent and conductive, and thus can be used as high-efficiency heat conductors or transparent nano-heaters for realizing thermally tunable/switchable silicon photonics devices. In particular, 2D materials can be easily transferred to silicon

photonic chips by a wet transfer method [65] or an imprint-transfer process [66]. In this case, there is no lattice match issue. More importantly, for silicon photonic devices with 2D materials, there is little mode mismatch between the active region with 2D materials and the passive region with pure silicon waveguides. As a result, silicon photonics with 2D materials is becoming more and more attractive for many applications.

In this paper, a review is given on hybrid silicon photonic devices with 2D materials. In section 2, we review the recent progresses on silicon-based photodetectors with 2D materials for the wavelength-bands from UV to mid-infrared (MIR), including normal-incident and waveguide-type photodetectors on silicon. In section 3, recent works on silicon photonic switches/modulators with 2D materials are summarized and discussed, including high-speed electro-optical modulators, high-efficiency thermal-optical switches and low-threshold all-optical modulators, etc. Finally, we give a discussion on the future work of silicon/2D material photonics.

2 Silicon-based photodetectors with 2D materials

Photodetectors are one of the widely used optoelectronic devices that can convert photons into an electrical signal. High-performance photodetectors play important roles in various modern optical systems. Traditional photodetectors are primarily based on bulk semiconductor materials, such as silicon [67], germanium [33, 34], and III-V semiconductors [68]. They usually work at room temperature for the wavelength range from visible to near-infrared (NIR). For MIR and FIR photodetection based on HgCdTe [69], InAs/InGaSb [70] and InSb [71], the photodetectors usually operate at liquid nitrogen temperature (77 K). Though traditional photodetectors have been developed successfully and been used widely, novel photodetectors based on 2D materials have also been demonstrated with fascinating properties, e. g., ultra-high carrier mobility, high responsivity, as well as broad wavelength-bands covering the range from UV to infrared (IR).

For 2D material photodetectors, there are several typical photocurrent generation mechanisms [72], such as the photothermal electric (PTE) effect, the photo-bolometric (PB) effect, the photoconductive (PC) effect and the photovoltaic (PV) effect. For the PV effect, the photo-generated electron-hole pairs are separated by the built-in electric field [73]. The photocurrent of the PTE effect is generated by an optically-induced temperature gradient

and is particularly efficient in combination with spatially varying doping of graphene [74]. The PB effect is based on the resistance change of the material due to the heating effect induced by light illumination [75]. For the PC effect, the resistance of the material is reduced because of increase of the free-carrier concentration [76]. The working mechanisms of the photodetectors can be switched or mixed by modifying the doping level of the 2D materials [75].

In the following part, we give a review for two types of silicon-based photodetectors with 2D materials. One is normal-incident 2D material photodetectors on silicon and the other one is silicon-based waveguide-type photodetectors with 2D materials.

2.1 Normal-incident 2D material photodetectors on silicon

Normal-incident photodetectors and the array are playing a key role in many fields of our daily life, such as electro-optical displays, imaging, environment monitoring, free-space optical communication, and military. In the past few years, normal-incident 2D material photodetectors on silicon have been extensively investigated and great progresses have been achieved with high speed as well as high responsivity for the wavelength range from UV to IR, as

summarized in Table 1. More details are reviewed below in sections 2.1.1 and 2.1.2.

2.1.1 UV/Visible photodetectors

As it is well known, UV photodetectors are very useful for the applications in military defense, environmental monitoring and UV astronomy. In order to realize UV photodetection, one way is to use wide-bandgap 2D materials, e. g., hexagonal boron nitride (hBN) with a bandgap as large as ~6 eV [187]. High-quality of hBN nanosheets can be synthesized by e. g., the pulsed laser plasma deposition (PLPD) technique [77, 78]. The photodetector demonstrated in [77] has a responsivity of 9 μA/W at zero bias. In [79], Ahmed et al. demonstrated a fast hBN-Si MSM photodetector operating with a very high bias voltage of 95 V.

As another popular direct-bandgap 2D material whose bandgap can be modified from ~0.3 to 2 eV [50, 51], BP has also been developed for realizing high-responsivity photodetection from near UV to NIR [80–82]. In Ref. [80], a near-UV BP photodetector shows a very high photoresponsivity of $\sim 9 \times 10^4$ A/W, which is five orders of magnitude higher than that for the visible-NIR light, due to the resonant-interband transition between two specially nested valence- and conduction-bands. As shown in [81], the responsivity for the BP photodetector working in the

Table 1: Summary of some normal-incident 2D material UV-visible photodetectors.

Year	Material	Wavelength	Mechanism	Responsivity	RT (BW)	IQE	EQE	Ref.
2012	Graphene	850 nm	PC	21 mA/W				[63]
2013	MoS$_2$	400–680 nm	PG	880 A/W	4 s			[82]
2014	Graphene/MoS$_2$	650 nm	PV PG	1.2×10^7 A/W		15%		[175]
2014	Graphene	400–900 nm	Schottky	10^7 V/W	1.2 ms		57%	[176]
2014	Graphene	UV − NIR	Tunneling	0.4–1.0 A/W	10^6 Hz	100%		[177]
2015	Graphene/Perovskite	400–800 nm	PG	180 A/W	87 ms		5×10^4%	[178]
2016	Graphene	200–1000 nm	PG	1000 A/W	400 ns		2.42×10^5%	[179]
2016	Graphene	300–1100 nm	Schottky	0.495 A/W	<25 ns 14 MHz	70–100%		[88]
2017	Graphene	200–400 nm	Schottky	>0.14 A/W	5 ns	>100%		[50]
2017	Graphene	UV − NIR MIR	PG	10^9 A/W 10 A/W	5 s	6×10^{10} 539	5×10^9 18	[55]
2018	Graphene	UV − 1100 nm	PG	500 A/W	240 μs		1.4×10^5%	[180]
2009	Graphene (2–3 layers)	1550 nm	PV	0.5 mA/W	40 GHz	6–16%		[18]
2010	Graphene (Bilayer)	1550 nm	PV	6.1 mA/W	16 GHz			[96]
2012	Graphene	600–1600 nm	PG	5×10^7 A/W	10–20 ms		25%	[58]
2013	Graphene	1535 nm	PC	0.6 mA/W		0.35%		[64]
2013	Graphene (3 layers)	514.5 nm	PTE	1×10^{-2} A/W				[85]
2014	Graphene	Visible − MIR	Tunneling/PG	>1 A/W	10–1000 Hz			[92]
2019	Graphene	532 nm 1550 nm	Tunneling	13 nA/mW 70 pA/mW			3×10^{-5} 5×10^{-8}	[181]
2016	BP	0.532–3.39 μm	PV PG	82 A/W	1.1 kHz			[99]

RT-rise time; BW-bandwidth; IQE-internal quantum efficiency; EQE-external quantum efficiency.

NIR region (i. e., 900 nm) can be improved to 7×10^6 A/W by lowering the temperature to 20 K. Some direct-bandgap transition metals dichalcogenides (TMDs), such as MoS_2 [83], WS_2 [84], WSe_2 [188], can also be used for photodetection. For example, a photoconductive MoS_2 photodetector [83] was fabricated [see Figure 1A] and exhibits a high responsivity of 880 A/W but long response time of ~9 s. With no illumination and without applying gate or drain bias, the device has a small Schottky barriers at the contacts. Increasing the gate voltage will lower the barriers at the contacts and work in ON state, which will increase the photoresponse due to the increased thermionic and tunneling currents. Operating in the OFF state brings the advantage of a reduced dark current.

As graphene has many unique properties, such as ultra-high carrier mobility (~200,000 $cm^2V^{-1}s^{-1}$) [49] at room temperature, broadband light absorption [42, 52, 53] and tunable Fermi level, several metal-graphene-metal (MGM)-type monolayer graphene photodetectors have been demonstrated for UV and NIR [75, 85]. However, the photo-responsivity is as low as several mA/W because there's only 2.3% light absorption for normal illuminated light. In order to enhance the light absorption of graphene for improving the responsivity, there are several popular approaches by using

e. g., optical microcavities [63, 64], the carrier-trapping effect [55–58], the plasmonic nanostructures [59–62]. As one of the most popular options, optical microcavities have been used widely by utilizing the resonance, e. g., Fabry–Perot cavities [63], photonic-crystal cavities [64], etc. On the other hand, the quality factor of the used optical cavity should be designed by making a trade-off between the optical bandwidth and the absorption enhancement. A second way for improving the responsivity is utilizing the carrier-trapping introduced by some wide-bandgap quantum-dots [55–58]. For example, for graphene-QDs photodetectors, the carrier trapping is mainly associated with the defects at the QD surface, and the un-paired electrons are transferred to graphene with a relatively long lifetime, which usually enables a high photoconductive gain. As shown in Figure 1B, a silicon-QDs/graphene hybrid phototransistor was demonstrated with a maximal responsivity of up to ~10^9 A/W in the wavelength range from UV to NIR [55]. This is because the photogenerated carriers in silicon-QDs are effectively separated due to the upward bending of the energy bands at the silicon-QD/graphene interface. One type of the carriers is trapped by defects (e. g., dangling bonds) at the QD surface, leading to the enhanced photo-response. In addition, for B-doped silicon-QDs, there is localized surface plasmon resonance in the MIR region,
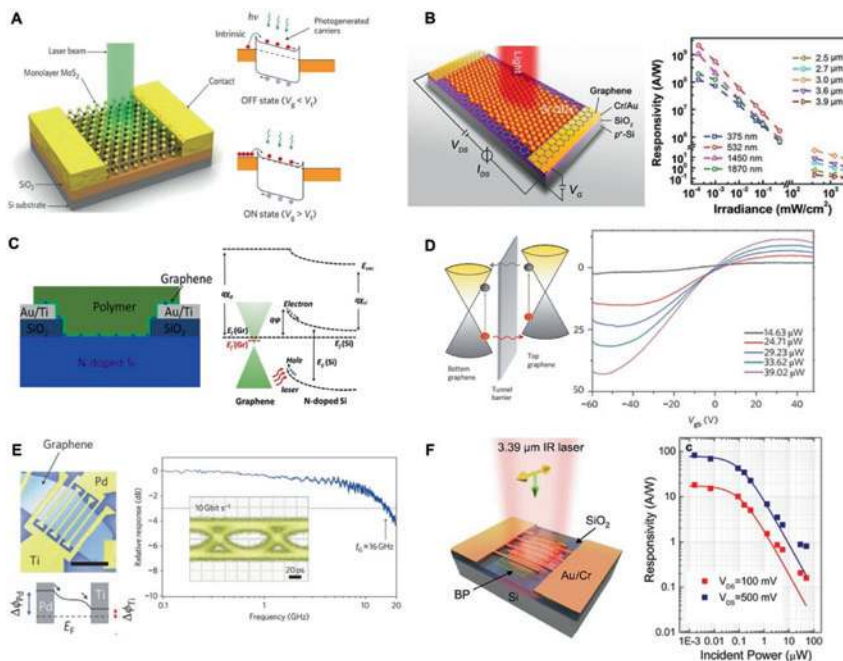

Figure 1: Normal-incident 2D material photodetectors on silicon. (A) A single-layer MoS_2 photodetector device working in the visible range. Photocurrent is generated under illumination and is the dominant channel current in the OFF state, while thermionic and tunneling currents contribute in the ON-state of the device. Reproduced with permission from [83]. Copyright 2013, Springer Nature. (B) A hybrid phototransistor based on B-doped Si QDs and graphene. The right figure shows the device responsivity as a function of laser irradiance at different wavelengths. Reproduced with permission from [55]. Copyright 2017, American Chemical Society. (C) A silicon-graphene conductive photodetector with a high responsivity. The band diagram of the graphene/N-doped silicon junction is shown in the right. Reproduced with permission from [89]. Copyright 2017, Springer Nature. (D) Ultra-broadband high responsivity graphene/Ta_2O_5/graphene tunneling photodetector.

Under light illumination, the electrons (gray) and holes (red) can transport through the tunneling barrier. Reproduced with permission from [92]. Copyright 2014, Springer Nature. (E) A high-speed MGM photodetector with asymmetric metal contacts. The graphene doping under Pd and Ti electrodes is different and photocurrent can flow in the same direction with appropriate gate voltage. Reproduced with permission from [96]. Copyright 2010, Springer Nature. (F) A BP photodetector at 3.39 μm. Reproduced with permission from [99]. Copyright 2016, American Chemical Society.

which enhances the light absorption of graphene and enables MIR photodetection. Similarly, ZnO–QDs have also been introduced to work together with graphene for achieving high responsivity in the UV region [56, 57]. As the third approach to enhance the responsivity, plasmonic nanostructures, such as nanoparticles [59–61] and nanostructures [62, 86], are often introduced to act as subwavelength scattering sources and nano-antennas, enabling high photoresponse at the corresponding plasmon resonance frequency. For example, in [86] gold-patched nanostructures were introduced for realizing an ultrafast (>50 GHz) graphene photodetector with a responsivity of 0.6 A/W at 800 nm.

In addition, Graphene/Si Schottky photodiodes are also suitable for UV and visible photodetection with the assistance of light absorption in the depleted silicon region. Here graphene acts as an optically transparent charge collector. The photogenerated carriers in the depleted silicon region can be separated effectively by the graphene/Si Schottky junction, enabling a high responsivity. In particular, the fabrication process is simple and the cost is low. Wan et al. fabricated a graphene/Si Schottky photodiodes at zero bias [87], exhibiting fast time response (5 ns), low dark current, as well as a responsivity of 0.14 A/W in the wavelength range of 200–400 nm. The built-in potential of the graphene/Si Schottky junction can be increased further by putting silicon QDs on top of graphene and the responsivity is enhanced to be 0.495 A/W [88]. Another high-responsivity silicon-graphene photodetector was also demonstrated by using a N-type silicon with a doping level of $\sim 7 \times 10^{15}$ cm^{-3} [89], as shown in Figure 1C. With this structure, when the laser illuminates the active region with a graphene/Si Schottky junction, the electron-hole pairs is generated in the depletion region in silicon and separated by the build-in field, and finally the electrons are transferred to the graphene sheet. The fabricated photodetector is able to detect an optical power as low as 6.2 pW at 635 nm with an ultra-high responsivity of 2.4×10^7 A/W. The corresponding rising time and decay time are about 32 and 60 μs, respectively, which is much faster than those quantum-dots/graphene photodetectors (~10 ms) [90].

2.1.2 Infrared photodetectors

NIR photodetectors are very important for various important applications, e. g., biological imaging (800–1100 nm) and optical communication (830/1310/1550 nm). Konstantatos et al. demonstrated a graphene-QD phototransistor with a responsivity up to 5×10^7 A/W in the 600–1600 nm wavelength range [58]. Note that zero-bandgap graphene photodetectors usually have a large dark current. When using the MoS$_2$-graphene-WSe$_2$ heterostructure for realizing photodetectors [91], the dark current and the noise power could be suppressed strongly and the wavelength range of 400–2400 nm is covered. As an alternative, the tunneling photodetectors have also been reported with relatively low dark current as well as a high responsivity [92–94]. For example, a graphene/Ta$_2$O$_5$/graphene photodetector [92] was demonstrated with a responsivity of >1 A/W from visible to midinfrared, as shown in Figure 1D. Here the top graphene layer was found to be more heavily p-doped than the bottom one, with an average Fermi energy difference of 0.12 eV. The tunneling barrier is tilted toward the bottom graphene layer in order to equilibrate the Fermi level, and favors hot electrons tunneling from the top graphene-layer to the bottom one when illuminated by light.

Regarding the applications in optical communication, it is desired to develop high-speed photodetectors. In 2009, Xia et al. demonstrated an ultrafast MGM photodetector at 1550 nm, showing a 3 dB-bandwidth of >40 GHz [95]. Later, they demonstrated another high-speed graphene photodetector with an improved responsivity of 6.1 mA/W (@1550 nm) generated by the PV effect [96], as shown in Figure 1E. In this design, asymmetric metallization scheme and interdigital metal fingers were used in order to create a large electric field by breaking the mirror symmetry of the built-in potential. TMDs have also been used for realizing photodetectors operating at the NIR region. For example, a MoS$_2$ photodetector was demonstrated with the help of plasmonic nanostructures [97]. When plasmonic nanostructures are excited by the NIR light, hot electrons with energy higher than the MoS$_2$-Au Schottky barrier are generated and injected from the gold layer to the MoS$_2$ layer for photocurrent generation. With this design, the responsivity is about 5.2 A/W at 1070 nm.

It is also possible realize the photodetection in the MIR range by using narrow-bandgap 2D materials, such as graphene and BP. Zhang et al. patterned the graphene sheet to be QD-like arrays [98], and then the defect midgap states band electron trapping centers are formed on the boundary and the surface of graphene QDs. The photodetector shows a broadband photoresponse from visible (532 nm) up to MIR (~10 μm) with a high responsivity. The structure with gold-patched graphene nano-strips even enables a very high responsivity of 11.5 A/W at the wavelength of 20 μm [86]. In [99], a 10-nm-thick BP photodetector exhibits a high responsivity up to 82 A/W in the 3.39 μm range, as shown in Figure 1F. The cutoff wavelength can be extended further to 7.7 μm by applying a vertical electrical field on the 5 nm-thick BP, as demonstrated in [100].

2.2 2D material waveguide photodetectors on silicon

It is well known that the absorption of graphene is only ~2.3% for normal incidence, which is quite limited for achieving high responsivity. Alternatively, the utilization of silicon photonic waveguides can greatly enhance the graphene absorption, owing to a long light-graphene interaction length. In addition, there is little mode mismatch between a hybrid silicon-graphene waveguide and a pure-silicon waveguide. Therefore, great efforts have been made to realize waveguide photodetectors for silicon photonics by introducing some 2D materials, e. g., graphene, BP, etc., as summarized in Table 2. In particular, the ultra-high carrier mobility in graphene makes it promising for the realization of high-speed waveguide photodetectors on silicon. In 2013, Gan et al. demonstrated an MGM-type waveguide photodetector with asymmetric metal electrodes [18], as shown in Figure 2A. The electrodes are placed asymmetrically at both sides of the waveguide to create a lateral metal-doped junction, which is helpful to separate the photogenerated electron-hole pairs at zero

bias. As a result, the realized photodetector has a decent responsivity of 0.1 A/W and a 3 dB-bandwidth of >20 GHz. Later, another MGM-type silicon-graphene waveguide photodetector with asymmetric metal electrodes was demonstrated for working with 50 Gbit/s OOK signals [101]. The bandwidth can be even extended to >76 GHz in a 6-inch wafer process line [102]. However, the cladding on top of the silicon core is relatively thick (~40 nm), which makes the interaction between the evanescent field and the graphene sheet weak, and thus the responsivity for these photodetectors is as low as several mA/W [102].

Generally speaking, there are two ways available to enhance the responsivity of the graphene photodetectors. One is to increase photoelectric conversion efficiency by e. g., increasing the applied voltage or tuning the graphene doping in the active region. However, the method of increasing the applied voltage is not a good option because the power consumption and the dark current increase accordingly. The other one is to enhance the light absorption in graphene by e. g., extending the length of the absorption region or enhancing the interaction between graphene and the waveguide mode. However, when the

Table 2: Summary of 2D material waveguide photodetectors on silicon.

| Year	Material	Type	Wavelength (μm)	Detector type	Bias (V)	Responsivity (A/W)	Bandwidth (GHz)	Ref.
2013	Graphene	Graphene-Si	Visible−2.75	Schottky	−1.5	0.13	/	[20]
2013	Graphene	MGM	1.55	PV	0	0.0157	>20	[18]
					1	0.1		
2013	Graphene	MGM	1.31−1.65	PV	0	0.03	18	[19]
2014	Graphene	MGM	1.55	PTE	0	7×10^{-3}	41	[101]
2014	Graphene	MGM	1.55	PTE	0	3.6×10^{-3}	7.7	[182]
				PV	0.4	0.057		
2015	BP	MSM	1.55	PV/PB	0.4	0.135	3	[111]
2015	Graphene	MGM	1.55	PTE	0	0.078	42	[103]
				PV	1.2	0.36		
2016	Graphene	MGM	1.55	PTE	0	0.035	65	[104]
				PC	0.3	0.076		
2016	Graphene	Graphene-Si	1.48−1.55	Schottky	4	8×10^{-4}	5	[183]
2016	Graphene	Graphene-Si	1.55	Schottky	1	0.085	/	[184]
					3	0.37		
2017	BP	MSM	1.55	PC/PB	1.5	10	0.15	[185]
2017	Graphene	MGM	1.55	PB	1	1×10^{-3}	76	[102]
2018	Graphene	MGM	1.55	PTE	0	0.048	18	[105]
				PC	0.4	0.17		
2018	Graphene	MGM	1.55	PB	−0.4	0.5	>110	[106]
2019	Graphene	Graphene-hBN-Graphene	1.55	Tunneling	10	0.24	28	[167]
2019	Graphene	MGM	1.55	PV	2.2	0.36	110	[107]
2019	Graphene	MGM	1.55	PTE	0	12.2 (V/W)	42	[109]
2019	BP	MSM	2	PV	0.4	0.307	1.33	[112]
2019	Graphene	MGM	1.55	PB/PC	0.3	0.4	>40	[108]
			2			0.07	>20	
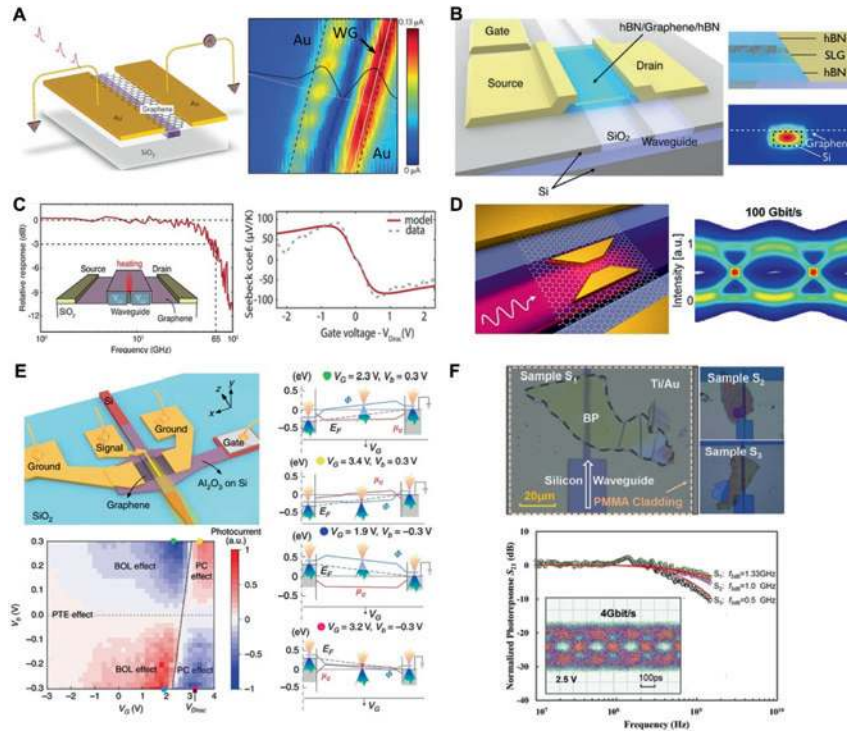
Figure 2: 2D material waveguide integrated photodetectors on silicon. (A) A waveguide-integrated graphene photodetector with asymmetric metal electrodes. Spatially resolved photocurrent (amplitude) image is measured at zero bias voltage, and a photocurrent profile plotted along the dashed white line is superposed on the image. Reproduced with permission from [18]. Copyright 2013, Springer Nature. (B) High-responsivity hBN/graphene/hBN photodetector on a buried silicon waveguide. Reproduced with permission from [103]. Copyright 2015, American Chemical Society. (C) A graphene photodetector integrated on a silicon slot-waveguide with a p–n junction. Right panel, calculated and measured Seebeck coefficient as a function of gate voltage. Reproduced with permission from [104]. Copyright 2016, American Chemical Society. (D) Plasmonically enhanced waveguide-integrated graphene photodetector. The optical field is enhanced at the edges and in the gap of the bowtie-shaped structures. Hundred Gbit/s OOK optical signal is realized with a double-layer graphene device. Reproduced with permission from [106]. Copyright 2018, American Chemical Society. (E) A silicon-graphene hybrid plasmonic waveguide photodetector for photodetection in 1.55 and 2 μm. The photocurrent map is measured as the gate voltage V_G and the bias voltage V_b varies. The calculated energy band diagram is shown in the right. Reproduced with permission from [108]. Copyright 2020, Springer Nature. (F) Microscope images for a hybrid silicon/BP waveguide photodetector at 2 μm. The 3 dB-bandwidth of the device is about 1.33 GHz and an improved eye-diagram with a bit rate of 4.0 Gbit/s is achieved by increasing the bias voltage to 2.5 V. Reproduced with permission from [112]. Copyright 2019, John Wiley and Sons.

absorption region length is extended, the device footprint and the capacitance will increase, which also prevents high-speed operation. As a result, in recent years people focus more on improving the responsivity by tuning the doping in the graphene active region and enhancing the light-graphene interaction.

In order to modifying the doping level in graphene, one can add a gate voltage appropriately. Shiue et al. proposed a high-responsivity graphene/boron-nitride waveguide photodetector for silicon photonics by introducing an additional gate electrode to tune the graphene Fermi level in the active region [103], as shown in Figure 2B. The graphene sheet is encapsulated in hBN, so that ultra-high mobility of graphene can be maintained well in the heterostructure. In addition, the contact resistance is reduced effectively by using the one-dimensional edge contact of graphene-hBN. In this device, the photocurrent is mainly generated by the PTE effect and is related to the Seebeck coefficient as well as the temperature gradient. Since the Seebeck coefficient is strongly depended on the carrier density and the chemical potential of graphene, it can be optimized by choosing the drain-source voltage and the

gate voltage appropriately. This hBN-graphene-hBN heterostructure photodetector demonstrated in [103] exhibits a large 3 dB-bandwidth of 42 GHz and a high responsivity of 0.36 A/W when operating at a 1.2 V bias voltage. In order to precisely control the doping-level in graphene, a silicon nano-slot waveguide was introduced to enable a dual gate for building a controllable p-n junction, as shown in Figure 2C [104]. In this design, the modal field is strongly confined and enhanced in the nano-slot. Furthermore, the graphene doping can be controlled by using dual gate voltage in order to form a desired Seebeck coefficient spatial distribution. In this case, a strong PTE effect was observed with a high responsivity of 36 mA/W at zero bias. As demonstrated in [105], the responsivity resulting from the PTE effect can be further enhanced to 48 mA/W when utilizing a photonic-crystal waveguide, in which case the Seebeck coefficient can be controlled in the entire graphene layer.

As it is well known, light absorption and responsivity can be enhanced further when using plasmonic waveguides with very strong field localization [106–109]. Pospischil et al. demonstrated a silicon-graphene waveguide photodetector

with a metal signal-electrode placed at the center of the waveguide [19]. With this structure, light absorption is enhanced and the photogenerated carriers can be separated effectively by the built-in potential at the metal-graphene interfaces. The achieved responsivity is about 30 mA/W for the monolayer-graphene case, while the responsivity can be increased to 50 mA/W when using bilayer-graphene. Recently another plasmonics-enhanced waveguide photo-detector was demonstrated with a 6 μm-long absorption region of graphene. This photodetector with structural symmetry works with the PB effect and exhibits a negative photocurrent with respect to the bias voltage. It shows a high operation speed, enabling 100 Gbit/s OOK and PAM4 data signal reception, as shown in Figure 2D. Even though the light-graphene interaction is enhanced greatly, one should notice that there is still a lot of unwanted absorption from metal in these traditional plasmonic waveguides, which greatly limits the responsivity.

More recently, an ultrafast silicon-graphene hybrid plasmonic waveguide photodetector was proposed and demonstrated for the wavelength bands of 1.55 μm and beyond [108], as shown in Figure 2E. In this design, a narrow metal strip (~200 nm) is placed on the top of the silicon waveguide ridge to achieve the field enhancement for increasing graphene absorption. In particular, the silicon waveguide ridge is very wide and ultra-thin, so that the graphene absorption is enhanced and the metal absorption is reduced. For the optimized structural design, the absorption coefficient in graphene is 0.23 dB/μm. Furthermore, a gate voltage is applied to optimize the graphene doping in the active region. The chemical potential for the graphene sheet underneath the gold electrodes is estimated to be −0.1 eV due to the pinning effect. When graphene is highly doped by appropriately applying the gate voltage, the bolometric coefficient is large and thus the PB effect is dominant. While graphene is lightly doped, the PB effect is suppressed and the lifetime of the photogenerated carriers becomes long and thus the PC effect becomes dominant. The fabricated photodetector exhibits a large 3-dB-bandwidth of >40 GHz (setup-limited) and a high responsivity of 0.4 A/W at a bias voltage of −0.3 V for the 1.55 μm wavelength-band. When operating at 2 μm, the device has a large setup-limited 3 dB-bandwidth of >20 GHz and a responsivity of 70 mA/W at a bias voltage of −0.3 V. It paves the way for realizing high-performance waveguide photodetectors at 1.55 μm and beyond for many applications, such as optical communications [37], on-chip spectroscopy, optical bio-sensing [40], and Lidar [110].

As it is well known, graphene photodetectors operating in the photoconductive mode usually have a dark current due to the zero-bandgap. When using graphene-silicon Schottky diode for the waveguide photodetector, the dark current and the noise can effectively be suppressed [20]. However, it works with a very slow speed of 2 MHz. As an alternative, BP has a direct bandgap of ~0.3 eV in bulk and 1.8–2 eV in monolayer [50, 51], enabling the photodetection for broadband photodetection. Furthermore, BP has a higher absorption than graphene. In [111], a BP waveguide photodetector was realized with a responsivity of 657 mA/W (@ 1550 nm) at a bias voltage of 2 V, and an experiment for receiving 3 Gbit/s data was demonstrated. More recently, hybrid silicon-BP waveguide photodetectors were also demonstrated for the wavelength-band of 2 μm [112], as shown in Figure 2F. For these devices, mechanically-exfoliated BP thin films are usually used and one should carefully choose the BP orientation and the BP thickness because of the anisotropic properties of BP [113–115]. A 90° orientation is desired for maximizing the BP absorption. For the BP photodetectors @ 2 μm demonstrated in [112], which are working with the photovoltaic (PV) effect dominantly, the measured responsivity is about 0.4 A/W and the bit rate for the data-receiving is up to 4 Gbit/s.

3 Silicon-based optical switches/ modulators with 2D materials

Optical switches and optical modulators are very important for realizing dynamic light manipulation for many systems. For example, it is desired to achieve high-speed, low power consumption optical switches and optical modulators on silicon for optical interconnects. Since the Fermi level of some 2D material can be tuned electrically, its complex refractive index can be modified accordingly and thus one can realize high-speed optical modulators potentially. Furthermore, regarding that some 2D materials are very transparent and conductive, it provides a good option to realize high-efficiency heat conductors or transparent heaters for thermally-switchable silicon photonics devices. In this section, we give a review on silicon photonic switches/modulators with 2D materials, including high-speed electro-optical modulators, high-efficiency thermal-optical switches, and low-threshold all-optical modulators, etc.

3.1 Efficient optical switches with 2D materials on silicon

Switchable/tunable silicon photonic devices are playing a very important role for all-optical signal routing and

switching in reconfigurable photonic networks/systems [116]. Because silicon has high thermo-optic coefficient ($\sim 1.8 \times 10^{-4}$/K @ $\lambda = 1.55\,\mu m$) and high thermal conductivity (~ 149 W/m·K) [117], utilizing the thermo-optic effect is one of the most popular approaches for realizing switchable/tunable silicon photonic devices. Traditionally, metal micro-heaters are introduced on the top of the phase-shifter for heat generation. In order to prevent light absorption of metal, a thick SiO_2 upper-cladding is usually introduced as an insulator. Unfortunately, SiO_2 has poor heat conductivity and thus the response speed and the heating efficiency become low. Besides, the silicon core is usually much colder than the metal heater, which limits the temperature dynamics of the silicon core because there is a limitation for the temperature of the metal heater itself. An integrated heater formed by doped silicon regions was introduced for low-power and high-speed thermal-tuning, as demonstrated in [118]. However, the fabrication process for the heater regions with different doping-levels is complicated. Therefore, it is still desired to develop a simple and efficient heating approach for thermally tunable/switchable silicon photonic devices. As it is well known, graphene is highly transparent and has an ultra-high intrinsic thermal conductivity (~ 5300 W/m·K at room temperature) [43, 119]. Furthermore, the flexibility of graphene is helpful when used for complex surfaces. Therefore, it is attractive to introduce graphene nano-structures for the heating management in silicon photonics [120–122].

For example, a graphene-based transparent heat conductor was used for thermally tunable silicon Mach-Zehnder interferometer (MZI), as shown in Figure 3A [120]. Here the graphene heat conductor covers the metal heater as well as a part of MZI arm, so that heat can be delivered from the metal heater to the MZI arm for light modulation. When the heating power $P_{heating}$ varies from 0 to 110 mW,

the spectral response has a red shift of ~ 7 nm. In order to realize more efficient heating, transparent graphene nano-heater was introduced, as shown in Figure 3B [123]. In this case, the graphene nano-heater is placed directly on the silicon core without any insulator. For the silicon microdisk resonator with the graphene nano-heater, the resonance wavelength can be shifted thermally with high efficiency. In the experiment, the spectral response has a redshift of ~ 5 nm with a heating power of 10.5 mW. When the radius of the microdisk is reduced to 2 μm, the heating efficiency is improved to as high as ~ 1.67 nm/mW. Later, Yan et al. demonstrated a slow-light silicon photonic-crystal waveguide with graphene microheater [124], as shown in Figure 3C, in which the tuning efficiency is about 1.07 nm/mW and the rise time is about 750 ns. In 2017, the graphene microheater was also used for silicon nanobeam cavity [125] and the heating efficiency is as high as 1.5 nm/mW in experiment because of the shrunk heating volume. For these thermally tunable optical cavities with graphene nano-heaters, one can realize an efficient thermo-optic switch for a fixed wavelength around the resonance, which is useful for low power-consumption reconfigurable silicon photonics in the future.

3.2 High-speed optical modulators with 2D materials on silicon

As one of the most important devices in optical communication systems, high-speed optical modulators have attracted intensive attention in the past years. Among various mechanisms for realizing fast optical modulation, the utilization of 2D materials is emerged as a new option. In particular, graphene has been very attractive because of its complex refractive index can be modulated
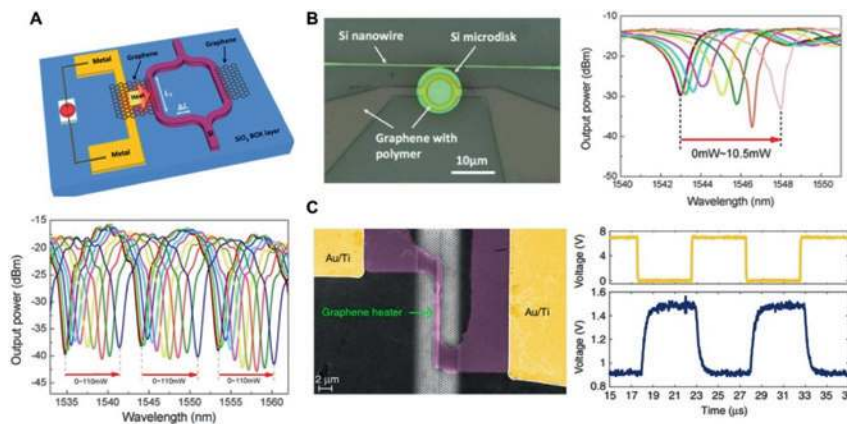

Figure 3: Graphene heaters on silicon waveguides. (A) A thermally-switchable MZI with a graphene transparent beat conductor and a non-local traditional metal heater. With the heating power varies from 0 to 110 mW, the spectral response has a red shift of ~ 7 nm. Reproduced with permission from [120]. Copyright 2014, AIP Publishing. (B) A thermally-switchable microdisk resonator with transparent graphene nano-heater. The spectral response has a redshift of ~ 5 nm with a heating power of 10.5 mW. Reproduced with permission from [123]. Copyright 2016, The Optical Society. (C) A slow-light-enhanced graphene microheater. The driving electrical signal (yellow) and corresponding temporal signal (blue) are shown in the right. Reproduced with permission from [124]. Copyright 2017, Springer Nature.
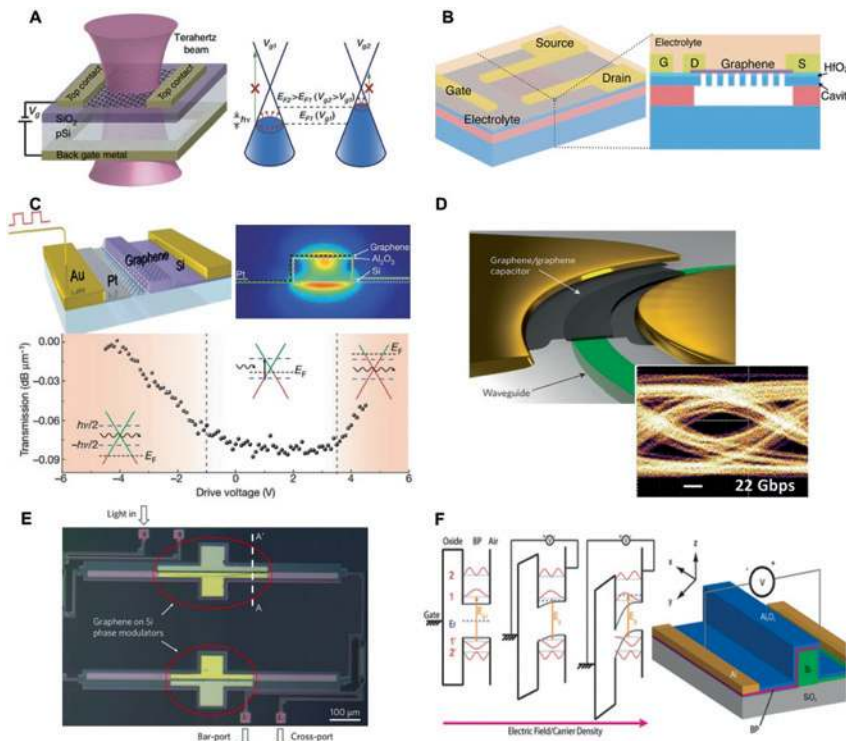
Figure 4: High-speed optical modulators with 2D materials on silicon. (A) A graphene free-space modulator at terahertz wavelength. By applying a voltage V_g, one can tune the density of states available for intraband transitions (red arrows), thus terahertz transmission. Reproduced with permission from [128]. Copyright 2012, Springer Nature. (B) A electrically controlled graphene-photonic crystal nanocavity modulator. Reproduced with permission from [135]. Copyright 2013, American Chemical Society. (C) First demonstrated broadband graphene-silicon waveguide integrated electrical-optical amplitude modulator. When the Fermi level (E_F) is lower than half the photon energy ($-hv/2$), there are no electrons available for the interband transition, and when the Fermi level (E_F) is higher than half the photon energy ($hv/2$), all electron states in resonance with incident photons (hv) are occupied, thus the transition is forbidden. Reproduced with permission from [17]. Copyright 2011, Springer Nature. (D) A high-speed GOG type graphene ring modulator based on Si_3N_4 waveguide. The open 22 Gbps non-return-to-zero (NRZ) eye diagram is realized. Reproduced with permission from [141]. Copyright 2015, Springer Nature. (E) A graphene-silicon integrated phase modulator with MZI structure. The top arm has a 400 μm graphene on silicon, while the bottom arm has 300 μm graphene on silicon. Reproduced with permission from [144]. Copyright 2018, Springer Nature. (F) Mid-infrared electro-optic modulator realized by using BP. Left figure shows energy band diagrams for 5 nm thick BP as electric field or carrier density varies. Reproduced with permission from [145]. Copyright 2016, American Chemical Society.

conveniently by tuning its electrical conductivity (or Fermi level) [126]. More importantly, graphene-based optical modulators can work in a very broad wavelength-band from the visible to the longwave infrared (even terahertz) range [46, 126, 127], which is extremely useful for many applications.

In Ref. [128], terahertz-wave modulation was demonstrated by electrically tuning the density of states available for intraband transitions in graphene, as shown in Figure 4A, and the intensity modulation depth is about 15%. Since graphene is atomically thin, the light–matter interaction is usually too weak to achieve large modulation depth. In order to enhance the interaction strength, various resonant and plasmonic structures [126] have been introduced, such as plasmonic antenna arrays [129–132], Fano resonant structures [133], metasurfaces [134], photonic-crystal cavities [135], and reflectors [136]. For example, the modulation depth is increased to 64% by adding a reflector under the graphene and optimizing substrate thickness so that the intensity of the terahertz-wave interference in graphene layer is at the maxima [136]. When using plasmonic structures fabricated on graphene, the interaction of

the incident optical field with the graphene sheet can be enhanced by localizing the optical fields strongly [137]. Several graphene modulators have been demonstrated by electrically controlling the damping of plasmonic resonances in the MIR [129–131] and terahertz ranges [132]. Not only the intensity but also the phase of the lightwave can be modulated by using graphene-assisted metamaterials with strong resonances [134]. As shown in Figure 4B, a silicon air-slot photonic-crystal cavity, enabling strong interaction between the graphene sheet and the resonant field, provides the modulation of the cavity reflection for a swing voltage of only 1.5 V [135].

As a simple approach to enhance the light–matter interaction, utilizing hybrid silicon-graphene waveguides is also popular for the realization of efficient optical modulators on silicon, as summarized in Table 3. In 2011, Liu et al. demonstrated the first GHz-level electrical-optical amplitude modulator with a hybrid silicon-graphene waveguide [17]. As shown in Figure 4C, the graphene sheet is placed on top of the silicon core, and there is a graphene-oxide-silicon (GOS) capacitance structure. When an external voltage is applied, the Fermi-level of graphene is

Table 3: Summary of high-speed optical modulators with 2D materials on silicon.

Year	Material	WG Type	MD (dB)	Optical BW (nm)	Electrical BW (GHz)	PC (fJ/bit)	Footprint (um²)	Drive Voltage (V)	Ref.
2011	Graphene	Straight	2.3	250	1	1200	25	4	[17]
2012	Graphene	Straight	6.5	250	1	1000	16	5	[138]
2015	Graphene	Ring Resonator	12.5	0.1	/	/	8000	8.8	[142]
2015	Graphene	Ring Resonator	15	0.1	30	800	5000	10	[141]
2016	Graphene	Straight	2	140	35	1400	18	25	[140]
2016	Graphene	Straight	2.5	>80	5.9	350	37.5	2.5	[139]
2017	Graphene	Plasmonic WG	2.1	>20	10^{-3}	/	2.4	7.5	[143]
2018	Graphene	MZI	35	/	5	1000	200	7.25	[144]
2019	Graphene	PhC	0.55	30	12	/	120	8	[186]

MD-modulation depth; PC-power consumption.

tuned and the interband graphene absorption can be modulated accordingly. The modulation depth can be enhanced significantly by using an improved design with graphene-oxide-graphene (GOG) capacitor [138]. Unfortunately, in this design the 3-dB-bandwidth is still limited to be about 1 GHz. In order to improve the modulation speed, Hu et al. proposed an improved structure design by introducing a doped silicon region to decrease the contact resistance and the silicon resistance [139]. In this way, a high-speed modulation of 10 Gbit/s was demonstrated. In [140], another high-speed GOG-type graphene modulator was demonstrated by introducing a 120-nm-thick Al_2O_3 insulation layer and the measured 3 dB bandwidth is as high as 35 GHz when operating at a high drive voltage of 25 V. As it is well known, micro-resonators are often used to enhance light–matter interaction and thus the active region can be shrunk [141, 142]. For example, Figure 4D shows a high-speed graphene modulator based on a silicon ring-resonator [141], which shows a 3 dB bandwidth of 30 GHz and a modulation depth of 15 dB when operating with a 10 V swing. When introducing plasmonic nano-slot waveguides, it is possible to enhance the light–matter interaction strongly due to the optical filed localization. As shown in [143], an efficient electro-optic modulation with an ultra-compact footprint was demonstrated.

Note that graphene can be also used to realize phase modulators because the real part of its complex refractive index can be tuned. In [144], a 10 Gbit/s graphene phase modulator integrated in an MZI was demonstrated, as shown in Figure 4E. This phase modulator exhibits an enhanced modulation efficiency of 0.28 V·cm, which is 5-fold improvement compared to the silicon MZI modulators based on p–n junctions. This paves a way for realization of complex modulation formats by using graphene phase modulators. More recently, BP has also been used for realizing optical modulation, as shown in Figure 4F [145]. In this case, when a positive gate bias is applied, the out-of-plane electric field leads to band-bending across the quantum well (QW), and thus the bandgap E_g is effectively reduced [201]. Such bandgap shrinkage can be described by the quantum-confined Franz-Keldysh (QCFK) effect [202] and leads to red-shift [145, 146], which is useful for MIR applications [147].

3.3 Low-threshold all-optical modulators with 2D materials on silicon

Graphene is a unique material with strong nonlinear optical effects, such as saturable absorption, and has attracted lots of intention in many applications of nonlinear photonics. As it is well known, graphene has one order of magnitude lower saturation intensity and 2–3 times higher modulation depth than single-walled carbon nanotubes (SWNTs) [148–150] and semiconductor saturable absorber mirrors (SESAMs) [151]. Thus, it is very promising to use graphene for realizing pulse lasers. Currently various fiber pulse lasers have been demonstrated [152–156]. For example, in [152] a graphene saturable absorber for ultrafast pulsed lasers was generated with an ultrashort pulse (~756 fs) in the communication band, as shown in Figure 5A. In the experiment, the optical intensity for saturable absorption is 0.61–0.71 MW/cm² for the graphene sheets with different layers. The wavelength-band of the mode-locked lasers can be extended to e. g., 1.94 μm [156]. Some other 2D materials have also been used as the saturable absorber. A mode-locked Er:ZBLAN fiber laser working at 2.8 μm was realized by using mechanically-exfoliated BP saturable absorber [157], and a MoS_2 mode-locked fiber laser was demonstrated under all-anomalous,
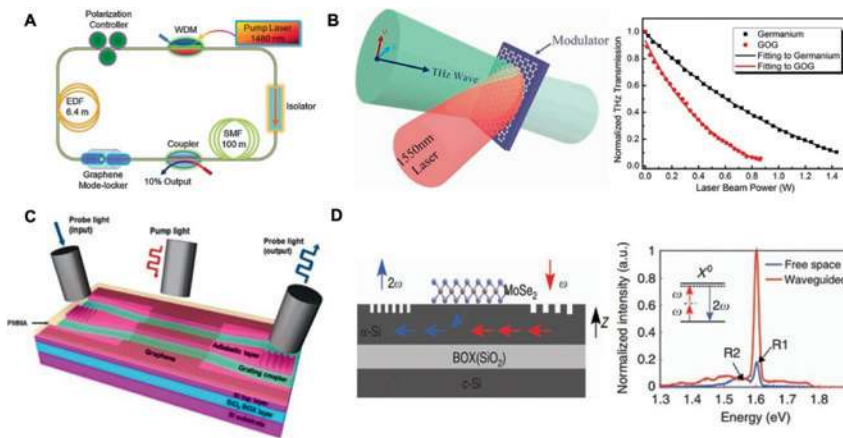
Figure 5: 2D material all-optical modulators. (A) An ultrafast pulsed laser with a graphene saturable absorber. Reproduced with permission from [152]. Copyright 2009, John Wiley and Sons. (B) An all-optical spatial terahertz modulator with a monolayer graphene sheet. The normalized THz transmission is given in right figure for both Ge substrate and graphene on Ge (GOG) structure. Reproduced with permission from [159]. Copyright 2014, Springer Nature. (C) A silicon-graphene all-optical modulator with optically induced transparency effects. The generated photocarriers is separated by the Schottky diode junction and the Fermi level in the graphene moves down, thus absorption in graphene is suppressed. Reproduced with permission from [162]. Copyright 2014, American Chemical Society. (D) A silicon waveguide grating with $MoSe_2$ for second-harmonic generation. The normalized emission spectra measured in the free space and in the waveguide are shown in the right. Reproduced with permission from [165]. Copyright 2017, Springer Nature.

near-zero, and all-normal cavity dispersion around 1600 nm [155].

In addition, all-optical modulators with graphene have also been realized. In [158], an ultra-fast all-optical modulator was demonstrated by using a graphene-cladded nano-fiber, which shows a very short response time of ~2 ps. Definitely, it is very attractive to realize on-chip all-optical modulation with 2D materials. Among various 2D materials used for all-optical modulation on silicon, graphene is one of the most popular materials. As shown in Figure 5B, efficient all-optical amplitude modulation of terahertz wave can be realized by using a controlled light to photodoping graphene [159]. Moreover, it is possible to achieve a modulation depth as high as 99% [160]. Shi et al. proposed a graphene-cladded silicon photonic-crystal cavity and realized all-optical tuning effectively [161]. In the experiment, a 3.5 nm shift of the resonance wavelength and a 20% quality factor change were observed for the graphene/silicon photonic–crystal cavity by focusing the control laser on the cavity. In particular, the laser power for the saturation absorption is nearly two orders of magnitude lower than that for monolayer graphene on silica [161].

Efficient all-optical modulator can also be realized by using a hybrid silicon-graphene waveguide because the light-graphene interaction can be enhanced strongly. In [162], local and nonlocal all-optical modulations are demonstrated with the optically-induced transparency (OIT) effect in a graphene-silicon hybrid waveguide, as shown in Figure 5C. In this structure, the graphene sheet contacts with the silicon core directly. When the modulated 635 nm laser illuminates the waveguide on the top, the transmission of the probe light (λ = 1560 nm) can be modulated accordingly. In this case, photo-carriers are

generated in the silicon core by the 635 nm laser illumination and then transport to the graphene sheet through the silicon-graphene junction. As a result, the carrier concentration in graphene is varied, which introduces the change of the complex refractive index of graphene. In particular, the required power density for the OIT effect is about 2 W/cm^2, which is five orders of magnitudes lower than the traditional saturated absorption in graphene. Such an OIT effect is promising to realize low power all-optical modulations in silicon photonics. Recently, an all-optical switch with a graphene-loaded plasmonic waveguides on silicon was demonstrated with an ultra-low switching energy of 35 fJ and ultra-fast switching time of 260 fs [163], which is attributed to the enhanced nonlinear absorption in graphene induced by the extremely strong light confinement in the plasmonic waveguide. The light-emitting properties of 2D TMDs were also modulated and enhanced when combined with silicon photonic waveguides. In [164], the directions and intensity of the photo-luminescence emission in a monolayer WSe_2 was demonstrated by using a silicon photonic waveguide-grating structure. The second-harmonic generation from monolayer $MoSe_2$ was also enhanced dramatically with the assistance of an optical waveguide [165], as shown in Figure 5D, which paves the way for on-chip light modulation. When exciting the monolayer $MoSe_2$, a five times enhancement of the emission signal at 1.6 eV is achieved by using an evanescent waveguide mode, as compared to the free-space excitation. In 2017, an all-optical modulation within a monolayer WS_2-cladded waveguide was realized, which shows the signal transmitting along the waveguide can be amplified and modulated by a co-propagated pumped laser [166]. It is expected more and more on-chip

all-optical modulators using novel silicon photonic waveguides with 2D materials will be achieved in the future.

4 Conclusion and outlook

In this paper, we have given a review on recent progresses of hybrid silicon photonic devices with 2D materials for photodetection and optical modulation for the wavelength-bands from UV to MIR. As demonstrated previously, 2D materials provide new opportunities for realizing various active photonic devices on silicon owing to their extraordinary optoelectronic properties. In particular, the light–matter interaction can be enhanced greatly and easily when merging 2D materials with silicon photonic waveguides and cavities. In this way, the interaction length between the 2D materials and the lightwave propagating along the waveguide can be extended very effectively, which is really important for realizing high-performance silicon photonic devices.

Currently, numerous high-responsivity and high-speed silicon/2D materials photodetectors have been demonstrated benefiting from high carrier mobility and broad wavelength band with high light absorption. On the other hand, more efforts are desired to improve the photodetectors further. For example, the photodetectors with 2D materials (e. g., graphene) usually have a large dark current, limiting the detection sensitivity. Alternatively, some other 2D materials with a finite bandgap and strong light–matter interaction are available, such as BP and MoS_2. However, their relatively low carrier mobility greatly limits their response speed. So far, the highest bandwidth of the reported TMD waveguide photodetectors is still below 1 GHz [189, 190]. A potential solution is stacking multiple 2D material sheets together by van der Waasls (vdW) integration. The vdW integration could enable artificial heterostructures and superlattices with atomically-clean and electronically-sharp interfaces between highly disparate materials [191]. Recently, Nicolaus et al. demonstrated a waveguide integrated $MoTe_2$-graphene vdW heterostructure photodetector [192], for which the responsivity is about 0.2 A/W at 1300 nm and the normalized photo-dark-current (NPDR) ratio is almost an order of magnitude than pure-graphene photodetectors due to the bandgap in $MoTe_2$. Moreover, the vertical $MoTe_2$-graphene heterostructure design minimizes the carrier transit path length in TMDs and enables a record measured bandwidth of >24 GHz. In addition to using 2D materials with finite bandgaps to suppress the dark current, another way is to introduce some tunneling barrier layer based on e. g., hBN. A graphene/BN/graphene heterostructure tunneling photodiode on a silicon nitride

waveguide was demonstrated with a high on/off current ratio of >10^4 at the telecom wavelength [167]. The device also exhibits a large bandwidth of 28 GHz. In addition, 2D/2D vdW heterostructures can provide a smooth surface that is relatively free of dangling bonds and charge traps [193]. Previously, the mobility of transferred graphene is about only a few thousand $cm^2\,V^{-1}\,s^{-1}$. By encapsulating graphene in a BN/graphene/BN vdW heterostructure, an ultrahigh carrier mobility of 140,000 $cm^2\,V^{-1}\,s^{-1}$ and up to 1,000,000 $cm^2\,V^{-1}\,s^{-1}$ can be achieved at room temperature and cryogenic temperature, respectively [194–196]. The 2D materials vdW integration could also enable creation of a designed potential landscape for electrons to live in, i. e. quantum wells (QWs). Withers et al. described LEDs made by stacking metallic graphene, insulating h-BN, and various TMD monolayers into complex but carefully designed sequences [197]. Currently the ability to physically assemble 2D materials into vdW heterostructure has offered vast flexibility for heterogeneous material integration and has considerably accelerated both fundamental studies and proof-of-concept demonstrations. It is still challenging to achieve scalable vdW integration of heterostructure-device arrays with high yield and throughput [191].

In the past years, high-speed optical modulators with 2D materials have also been developed successfully. However, it is still very hard to improve the modulation speed further to 100 Gbps, which is desired for the future high-capacity optical interconnects. Furthermore, the insertion loss for these optical modulators is usually high, which is a big challenge for the real applications. 2D materials might also be useful for transparent nano-heaters in the switchable/tunable silicon photonic devices because of the transparency and high thermal/electrical conductivity. In particular, transparent graphene nano-heaters have been developed successfully for silicon photonic cavities, while the challenge is to further reduce the material absorption as well as the power consumption for switching/tuning. In addition to these optoelectronic devices, 2D materials all-optical devices on silicon are also attractive because many 2D materials also show strong optical nonlinearity. The saturable absorption in 2D materials (such as graphene, MoS_2, $MoSe_2$, WS_2, and WSe_2) is promising for realizing Q-switched lasers [168] or mode lock lasers [169, 170]. It is also possible to realize optical power limiters [171], frequency conversion [172, 173], and single-photon emitters [174] by using 2D materials.

Even though 2D materials work well in the long-wavelength region, another challenge for hybrid silicon photonic devices with 2D materials is that the SOI platform is not suitable for the applications beyond 3.5 μm due to the high absorption loss in silica [198]. One of the possible solutions

is using Ge-on-Si waveguide to achieve low-loss light transmission in MIR [199, 200] because Ge is an ideal material exhibiting high transparency over the entire MIR range (up to ~14 μm) almost [198]. Definitely, 2D materials are usually flexible and can be transferred to an arbitrary substrate by using the wet-transfer method [65] or the imprint transfer method [66]. Therefore, it is promising to develop photodetection and optical modulation in the MIR range by merging the Ge-on-Si waveguide with 2D materials.

As a summary, currently it is becoming very promising to develop silicon photonics by introducing 2D materials, so that the drawbacks of silicon itself can be compensated. More importantly, there is no lattice-mismatching and mode-mismatching when combining 2D materials with silicon photonics. Thus, the compatibility of the fabrication process and the structural design is very excellent for hybrid silicon photonic devices. More efforts to realize improved active silicon photonic devices with large-scale photonic integrated circuits on silicon can be expected in the future.

References

[1] K. Bergman, "Silicon photonics for high performance interconnection networks,"Optical Fiber Communication Conference, *Opt. Soc. Am.*, p. Tu3F.1, 2018.

[2] M. A. Taubenblatt, "Optical interconnects for high-performance computing," *J. Lightwave Technol.*, vol. 30, pp. 448–457, 2011.

[3] R. Soref, "The past, present, and future of silicon photonics," *IEEE J. Sel. Top Quantum Electron.*, vol. 12, pp. 1678–1687, 2006.

[4] D. Thomson, A. Zilkie, J. E. Bowers, et al., "Roadmap on silicon photonics," *J. Optics*, vol. 18, 2016, Art no. 073003.

[5] D. Liu, H. Wu, and D. Dai, "Silicon multimode waveguide grating filter at 2 μm," *J. Lightwave Technol.*, vol. 37, pp. 2217–2222, 2019, https://doi.org/10.1109/JLT.2019.2900439.

[6] D. Liu and D. Dai, "Silicon-based polarization-insensitive optical filter with dual-gratings," *Opt. Express*, vol. 27, pp. 20704–20710, 2019, https://doi.org/10.1364/OE.27.020704.

[7] S. Chen, H. Wu, and D. Dai, "High extinction-ratio compact polarisation beam splitter on silicon," *Electron. Lett.*, vol. 52, pp. 1043–1045, 2016, https://doi.org/10.1049/el.2016.0683.

[8] Y. Yin, Z. Li, and D. Dai, "Ultra-broadband polarization splitter-rotator based on the mode evolution in a dual-core adiabatic taper," *J. Lightwave Technol.*, vol. 35, pp. 2227–2233, 2017, https://doi.org/10.1109/JLT.2017.2662200.

[9] S. Wang, X. Feng, S. Gao, et al., "On-chip reconfigurable optical add-drop multiplexer for hybrid wavelength/mode-division-multiplexing systems" *Opt. Lett.*, vol. 42, pp. 2802–2805, 2017, https://doi.org/10.1364/OL.42.002802.

[10] C. Li, D. Liu, and D. Dai, "Multimode silicon photonics," *Nanophotonics*, vol. 8, pp. 227–247, 2018, https://doi.org/10.1515/nanoph-2018-0161.

[11] N. Youngblood and M. Li, "Integration of 2D materials on a silicon photonics platform for optoelectronics applications," *Nanophotonics*, vol. 6, pp. 1205–1218, 2017.

[12] D. Dai, Y. Yin, L. Yu, et al., "Silicon-plus photonics" *Front. Optoelectron.*, vol. 9, pp. 436–449, 2016, https://doi.org/10.1007/s12200-016-0629-9.

[13] X. Guan, H. Wu, and D. Dai, "Silicon hybrid nanoplasmonics for ultra-dense photonic integration," *Front. Optoelectron.*, vol. 7, pp. 300–319, 2014.

[14] A. W. Fang, H. Park, O. Cohen, et al., "Electrically pumped hybrid AlGaInAs-silicon evanescent laser," *Opt. Express*, vol. 14, pp. 9203–9210, 2006, https://doi.org/10.1364/oe.14.009203.

[15] H. Park, Y. Kuo, A. W. Fang, et al., "A hybrid AlGaInAs-silicon evanescent preamplifier and photodetector," *Opt. Express*, vol. 15, pp. 13539–13546, 2007, https://doi.org/10.1364/oe.15.013539.

[16] Y. Ishikawa, K. Wada, D. D. Cannon, et al., "Strain-induced band gap shrinkage in Ge grown on Si substrate," *Appl. Phys. Lett.*, vol. 82, pp. 2044–2046, 2003, https://doi.org/10.1063/1.1564868.

[17] M. Liu, X. Yin, E. Ulin-Avila, et al., "A graphene-based broadband optical modulator," *Nature*, vol. 474, pp. 64–67, 2011, https://doi.org/10.1038/nature10067.

[18] X. Gan, R. J. Shiue, Y. Gao, et al., "Chip-integrated ultrafast graphene photodetector with high responsivity," *Nat. Photon.*, vol. 7, pp. 883–887, 2013, https://doi.org/10.1038/nphoton.2013.253.

[19] A. Pospischil, M. Humer, M. M. Furchi, et al., "CMOS-compatible graphene photodetector covering all optical communication bands," *Nat. Photon.*, vol. 7, pp. 892–896, 2013, https://doi.org/10.1038/nphoton.2013.240.

[20] X. Wang, Z. Cheng, K. Xu, et al., "High-responsivity graphene/silicon-heterostructure waveguide photodetectors," *Nat. Photon.*, vol. 7, pp. 888–891, 2013, https://doi.org/10.1038/nphoton.2013.241.

[21] C. Koos, P. Vorreau, T. Vallaitis, et al., "All-optical high-speed signal processing with silicon–organic hybrid slot waveguides," *Nat. Photon.*, vol. 3, pp. 216–219, 2009, https://doi.org/10.1038/nphoton.2009.25.

[22] A. Melikyan, L. Alloatti, A. Muslija, et al., "High-speed plasmonic phase modulators," *Nat. Photon.*, vol. 8, pp. 229–233, 2014, https://doi.org/10.1038/nphoton.2014.9.

[23] M. C. Tien, T. Mizumoto, P. Pintus, et al., "Silicon ring isolators with bonded nonreciprocal magneto-optic garnets," *Opt. Express*, vol. 19, pp. 11740–11745, 2011, https://doi.org/10.1364/OE.19.011740.

[24] W. De Cort, J. Beeckman, T. Claes, et al., "Wide tuning of silicon-on-insulator ring resonators with a liquid crystal cladding," *Opt. Lett.*, vol. 36, pp. 3876–3878, 2011, https://doi.org/10.1364/OL.36.003876.

[25] G. Roelkens, L. Liu, D. Liang, et al., "III-V/silicon photonics for on-chip and intra-chip optical interconnects," *Laser Photon Rev.*,

vol. 4, pp. 751–779, 2010, https://doi.org/10.1002/lpor. 200900033.

[26] S. Chen, W. Li, J. Wu, et al., "Electrically pumped continuous-wave III–V quantum dot lasers on silicon," *Nat. Photon.*, vol. 10, pp. 307–311, 2016, https://doi.org/10.1038/nphoton. 2016.21.

[27] I. S. Chung and J. Mørk, "Silicon-photonics light source realized by III–V/Si-grating-mirror laser," *Appl. Phys. Lett.*, vol. 97, pp. 151113, 2010, https://doi.org/10.1063/1.3503966.

[28] H. T. Chen, P. Verheyen, P. De Heyn, et al., "High-responsivity low-voltage 28-Gb/s Ge pin photodetector with silicon contacts," *J. Lightwave Technol.*, vol. 33, pp. 820–824, 2014, https://doi.org/10.1109/JLT.2014.2367134.

[29] S. Liao, N. N. Feng, D. Feng, et al., "36 GHz submicron silicon waveguide germanium photodetector," *Opt. Express*, vol. 19, pp. 10967–10972, 2011, https://doi.org/10.1364/OE.19.01096.

[30] F. Y. Gardes, D. J. Thomson, N. G. Emerson, et al., "40 Gb/s silicon photonics modulator for TE and TM polarisations," *Opt. Express*, vol. 19, pp. 11804–11814, 2011, https://doi.org/10. 1117/12.874715.

[31] P. Dong, S. Liao, D. Feng, et al., "Low Vpp, ultralow-energy, compact, high-speed silicon electro-optic modulator," *Opt. Express*, vol. 17, pp. 22484–22490, 2009, https://doi.org/10. 1364/OE.17.022484.

[32] Y. B. Bolkhovityanov and O. P. Pchelyakov, "GaAs epitaxy on Si substrates: modern status of research and engineering," *Phys. Uspekhi*, vol. 51, pp. 437, 2008, https://doi.org/10.3367/UFNr. 0178.200805b.0459.

[33] J. Wang and S. Lee, "Ge-photodetectors for Si-based optoelectronic integration," *Sensors*, vol. 11, pp. 696–718, 2011, https://doi.org/10.3390/s110100696.

[34] J. Michel, J. Liu, and L. C. Kimerling, "High-performance Ge-on-Si photodetectors," *Nat. Photon.*, vol. 4, pp. 527–534, 2010, https://doi.org/1038/nphoton.2010.157.

[35] X. Fu, J. Cheng, Q. Huan, et al., "5 x 20 Gb/s heterogeneously integrated III-V on silicon electro-absorption modulator array with arrayed waveguide grating multiplexer," *Opt. Express*, vol. 23, pp. 18686–18693, 2015, https://doi.org/10.1364/OE.23. 018686.

[36] M. Rouvière, L. Vivien, X. Le Roux, et al., "Ultrahigh speed germanium-on-silicon-on-insulator photodetectors for 1.31 and 1.55 μm operation," *Appl. Phys. Lett.*, vol. 87, pp. 231109, 2005, https://doi.org/10.1063/1.2139837.

[37] R. Soref, "Group IV photonics: enabling 2 μm communications," *Nat. Photon.*, vol. 9, pp. 358–359, 2015, https://doi.org/10. 1038/nphoton.2015.87.

[38] B. Kuyken, X. Liu, R. M. Osgood, et al., "Mid-infrared to telecom-band supercontinuum generation in highly nonlinear silicon-on-insulator wire waveguides," *Opt. Express*, vol. 19, pp. 20172–20181, 2011, https://doi.org/10.1364/OE.19.020172.

[39] J. Sun, E. Timurdogan, A. Yaacobi, et al., "Large-scale nanophotonic phased array," *Nature*, vol. 493, pp. 195–199, 2013, https://doi.org/10.1038/nature11727.

[40] W. C. Lai, S. Chakravarty, Y. Zou, et al., "Silicon nano-membrane based photonic crystal microcavities for high sensitivity bio-sensing," *Opt. Lett.*, vol. 37, pp. 1208–1210, 2012, https://doi. org/10.1364/OL.37.001208.

[41] T. Hu, B. Dong, X. Luo, et al., "Silicon photonic platforms for mid-infrared applications," *Photon Res.*, vol. 5, pp. 417–430, 2017, https://doi.org/10.1364/PRJ.5.000417.

[42] F. Xia, H. Wang, D. Xiao, et al., "Two-dimensional material nanophotonics," *Nat. Photon*, vol. 8, pp. 899–907, 2014.

[43] A. A. Balandin, S. Ghosh, W. Bao, et al., "Superior thermal conductivity of single-layer graphene," *Nano Lett.*, vol. 8, pp. 902–907, 2008, https://doi.org/10.1021/nl0731872.

[44] R. R. Nair, P. Blake, A. N. Grigorenko, et al., "Fine structure constant defines visual transparency of graphene," *Science*, vol. 320, pp. 1308, 2008, https://doi.org/10.1126/science. 1156965.

[45] Y. Tang and K. F. Mak, "Nanomaterials: 2D materials for silicon photonics," *Nat. Nanotechnol.*, vol. 12, pp. 1121–1122, 2017, https://doi.org/10.1038/nnano.2017.230.

[46] Z. Sun, A. Martinez, and F. Wang, "Optical modulators with 2D layered materials," *Nat. Photon.*, vol. 10, pp. 227–238, 2016, https://doi.org/10.1038/nphoton.2016.15.

[47] K. S. Novoselov, A. Mishchenko, A. Carvalho, et al., "2D materials and van der Waals heterostructures," *Science*, vol. 353, 2016, Art no. aac9439, https://doi.org/110.1126/science. aac9439.

[48] R. Mas-Balleste, C. Gomez-Navarro, J. Gomez-Herrero, et al., "2D materials: to graphene and beyond," *Nanoscale*, vol. 3, pp. 20–30, 2011, https://doi.org/10.1039/c0nr00323a.

[49] K. Bolotin, K. Sikes, Z. Jiang, et al., "Ultrahigh electron mobility in suspended graphene," *Solid State Commun.*, vol. 146, pp. 351–355, 2008, https://doi.org/10.1016/j.ssc.2008.02.024.

[50] L. Li, Y. Yu, G. J. Ye, et al., "Black phosphorus field-effect transistors," *Nat. Nanotechnol.*, vol. 9, pp. 372–377, 2014, https://doi.org/10.1038/nnano.2014.35.

[51] H. Liu, A. T. Neal, Z. Zhu, et al., "Phosphorene: an unexplored 2D semiconductor with a high hole mobility," *ACS Nano*, vol. 8, pp. 4033–4041, 2014, https://doi.org/10.1021/nn501226z.

[52] A. C. Ferrari, F. Bonaccorso, V. Fal'Ko, et al., "Science and technology roadmap for graphene, related two-dimensional crystals, and hybrid systems," *Nanoscale*, vol. 7, pp. 4598–4810, 2015, https://doi.org/10.1039/C4NR01600A.

[53] F. Bonaccorso, Z. Sun, T. Hasan, et al., "Graphene photonics and optoelectronics," *Nat. Photon.*, vol. 4, pp. 611–622, 2010, https://doi.org/10.1038/nphoton.2010.186.

[54] K. F. Mak, M. Y. Sfeir, Y. Wu, et al., "Measurement of the optical conductivity of graphene," *Phys. Rev. Lett.*, vol. 101, pp. 196405, 2008, https://doi.org/10.1103/PhysRevLett.101.196405.

[55] Z. Ni, L. Ma, S. Du, et al., "Plasmonic silicon quantum dots enabled high-sensitivity ultrabroadband photodetection of graphene-based hybrid phototransistors," *ACS Nano*, vol. 11, pp. 9854–9862, 2017, https://doi.org/10.1021/acsnano.7b03569.

[56] W. Guo, S. Xu, Z. Wu, et al., "Oxygen-assisted charge transfer between ZnO quantum dots and graphene," *Small*, vol. 9, pp. 3031–3036, 2013, https://doi.org/10.1002/smll. 201370110.

[57] D. Ick Son, H. Yeon Yang, T. Whan Kim, et al., "Photoresponse mechanisms of UV photodetectors based on colloidal ZnO quantum dot-graphene nanocomposites," *Appl. Phys. Lett.*, vol. 102, pp. 021105, 2013, https://doi.org/10.1063/1.4776651.

[58] G. Konstantatos, M. Badioli, L. Gaudreau, et al., "Hybrid graphene–quantum dot phototransistors with ultrahigh gain," *Nat. Nanotechnol.*, vol. 7, pp. 363–368, 2012, https://doi.org/ 10.1038/nnano.2012.60.

[59] Y. Liu, R. Cheng, L. Liao, et al., "Plasmon resonance enhanced multicolour photodetection by graphene," *Nat. Commun.*, vol. 2, pp. 579, 2011, https://doi.org/10.1038/ncomms1589.

[60] F. Schedin, E. Lidorikis, A. Lombardo, et al., "Surface-enhanced Raman spectroscopy of graphene," *ACS Nano*, vol. 4, pp. 5617–5626, 2010.

[61] J. Mertens, A. L. Eiden, D. O. Sigle, et al., "Controlling subnanometer gaps in plasmonic dimers using graphene," *Nano Lett.*, vol. 13, pp. 5033–5038, 2013, https://doi.org/10.1021/nl4018463.

[62] T. J. Echtermeyer, L. Britnell, P. K. Jasnos, et al., "Strong plasmonic enhancement of photovoltage in graphene," *Nat. Commun.*, vol. 2, pp. 458, 2011, https://doi.org/10.1038/ncomms1464.

[63] M. Furchi, A. Urich, A. Pospischil, et al., "Microcavity-integrated graphene photodetector," *Nano Lett.*, vol. 12, pp. 2773–2777, 2012, https://doi.org/10.1021/nl204512x.

[64] R. J. Shiue, X. Gan, Y. Gao, et al., "Enhanced photodetection in graphene-integrated photonic crystal cavity," *Appl. Phys. Lett.*, vol. 103, pp. 241109, 2013, https://doi.org/10.1063/1.4839235.

[65] X. Li, Y. Zhu, W. Cai, et al., "Transfer of large-area graphene films for high-performance transparent conductive electrodes," *Nano Lett.*, vol. 9, pp. 4359–4363, 2009, https://doi.org/10.1021/nl902623y.

[66] R. A. Hemnani, J. P. Tischler, C. Carfano, et al., "2D material printer: a deterministic cross contamination-free transfer method for atomically layered materials," *2D Mater.*, vol. 6, pp. 015006, 2018.

[67] M. K. Lee, C. H. Chu, Y. H. Wang, et al., "1.55-μm and infrared-band photoresponsivity of a Schottky barrier porous silicon photodetector," *Opt. Lett.*, vol. 26, pp. 160–162, 2001, https://doi.org/10.1364/OL.26.000160.

[68] P. R. A. Binetti, X. J. M. Leijtens, T. De Vries, et al., "InP/InGaAs photodetector on SOI photonic circuitry," *IEEE Photon. J.*, vol. 2, pp. 299–305, 2010, https://doi.org/10.1109/JPHOT.2010.2046151.

[69] A. Rogalski, "HgCdTe infrared detector material: history, status and outlook," *Rep. Progress Phys.*, vol. 68, pp. 2267, 2005, https://doi.org/10.1088/0034-4885/68/10/R01.

[70] C. H. Grein, P. M. Young, M. E. Flatté, et al., "Long wavelength InAs/InGaSb infrared detectors: optimization of carrier lifetimes," *J. Appl. Phys.*, vol. 78, pp. 7143–7152, 1995, https://doi.org/10.1063/1.360422.

[71] I. Kimukin, N. Biyikli, T. Kartaloglu, et al., "High-speed InSb photodetectors on GaAs for mid-IR applications," *IEEE J. Sel. Top. Quantum Electron*, vol. 10, pp. 766–770, 2004.

[72] F. H. L. Koppens, T. Mueller, P. Avouris, et al., "Photodetectors based on graphene, other two-dimensional materials and hybrid systems," *Nat. Nanotechnol.*, vol. 9, pp. 780–793, 2014, https://doi.org/10.1038/nnano.2014.215.

[73] E. C. Peters, E. J. H. Lee, M. Burghard, et al.,"Gate dependent photocurrents at a graphene pn junction," *Appl. Phys. Lett.*, vol. 97, pp. 193102, 2010, https://doi.org/10.1063/1.3505926.

[74] X. Xu, N. M. Gabor, J. S. Alden, et al., "Photo-thermoelectric effect at a graphene interface junction. *Nano Lett.*, vol. 10, pp. 562–566, 2010, https://doi.org/10.1021/nl903451y.

[75] M. Freitag, T. Low, F. Xia, et al., "Photoconductivity of biased graphene. *Nat. Photon*, vol. 7, pp. 53–59, 2013, https://doi.org/10.1038/nphoton.2012.314.

[76] Z. Chen, Z. Cheng, J. Wang, et al., "High responsivity, broadband, and fast graphene/silicon photodetector in photoconductor mode," *Adv. Optical Mater.*, vol. 3, pp. 1207–1214, 2015, https://doi.org/10.1021/acsphotonics.8b00247.

[77] M. Rivera, R. Velázquez, A. Aldalbahi, et al., "High operating temperature and low power consumption boron nitride nanosheets based broadband UV photodetector," *Sci. Rep*, vol. 7, pp. 42973, 2017, https://doi.org/10.1038/srep42973.

[78] A. F. Zhou, A. Aldalbahi, and P. Feng, "Vertical metal-semiconductor-metal deep UV photodetectors based on hexagonal boron nitride nanosheets prepared by laser plasma deposition," *Opt. Mater. Express*, vol. 6, pp. 3286–3292, 2016, https://doi.org/10.3390/nano7120454.

[79] K. Ahmed, R. Dahal, A. Weltz, et al., "Growth of hexagonal boron nitride on (111) Si for deep UV photonics and thermal neutron detection," *Appl. Phys. Lett.*, vol. 109, pp. 113501, 2016, https://doi.org/10.1063/1.4962831.

[80] J. Wu, G. K. W. Koon, D. Xiang, et al., "Colossal UV photoresponsivity of few-layer black phosphorus," *ACS Nano*, vol. 9, pp. 8070–8077, 2015, https://doi.org/10.1021/acsnano.5b01922.

[81] M. Huang, M. Wang, C. Chen, et al., "Broadband black-phosphorus photodetectors with high responsivity," *Adv. Mater.*, vol. 28, pp. 3481–3485, 2016, https://doi.org/10.1002/adma.201506352.

[82] M. Buscema, D. J. Groenendijk, S. I. Blanter, et al., "Fast and broadband photoresponse of few-layer black phosphorus field-effect transistors," *Nano Lett.*, vol. 14, pp. 3347–3352, 2014, https://doi.org/10.1021/nl5008085.

[83] O. Lopez-Sanchez, D. Lembke, M. Kayci, et al., "Ultrasensitive photodetectors based on monolayer MoS_2," *Nat. Nanotechnol.*, vol. 8, pp. 497–501, 2013, https://doi.org/10.1038/nnano.2013.100.

[84] N. Perea-López, A. L. Elías, A. Berkdemir, et al., "Photosensor device based on few-layered WS_2 films," *Adv. Funct. Mater.*, vol. 23, pp. 5511–5517, 2013, https://doi.org/10.1002/adfm.201300760.

[85] M. Freitag, T. Low, and P. Avouris, "Increased responsivity of suspended graphene photodetectors," *Nano Lett.*, vol. 13, pp. 1644–1648, 2013, https://doi.org/10.1021/nl4001037.

[86] S. Cakmakyapan, P. K. Lu, A. Navabi, et al., "Gold-patched graphene nano-stripes for high-responsivity and ultrafast photodetection from the visible to infrared regime," *Light Sci. Appl.*, vol. 7, pp. 20, 2018, https://doi.org/10.1038/s41377-018-0020-2.

[87] X. Wan, Y. Xu, H. Guo, et al., "A self-powered high-performance graphene/silicon UV photodetector with ultra-s/allow junction: breaking the limit of silicon?" *npj 2D Mater. Appl.*, vol. 1, pp. 4, 2017, https://doi.org/10.17863/CAM.9667.

[88] T. Yu, F. Wang, Y. Xu, et al., "Graphene coupled with silicon quantum dots for high-performance bulk-silicon-based Schottky-junction photodetectors," *Adv. Mater.*, vol. 28, pp. 4912–4919, 2016, https://doi.org/10.1002/adma.201506140.

[89] J. Liu, Y. Yin, L. Yu, et al., "Silicon-graphene conductive photodetector with ultra-high responsivity," *Sci. Rep.*, vol. 7, pp. 40904, 2017, https://doi.org/10.1038/srep40904.

[90] G. Konstantatos, M. Badioli, Gaudreau, et al., "Hybrid graphene–quantum dot phototransistors with ultrahigh gain," *Nat. Nanotechnol.*, vol. 7, pp. 363–368, 2012.

[91] M. Long, E. Liu, P. Wang, et al., "Broadband photovoltaic detectors based on an atomically thin heterostructure," *Nano Lett.*, vol. 16, pp. 2254–2259, 2016, https://doi.org/10.1021/acs.nanolett.5b04538.

[92] C. H. Liu, Y. C. Chang, T. B. Norris, et al.,"Graphene photodetectors with ultra-broadband and high responsivity at room temperature," *Nat. Nanotechnol.*, vol. 9, pp. 273–278, 2014, https://doi.org/10.1038/nnano.2014.31.

[93] Q. Ma, T. I. Andersen, N. L. Nair, et al., "Tuning ultrafast electron thermalization pathways in a van der Waals heterostructure," *Nat. Phys.*, vol. 12, pp. 455–459, 2016, https://doi.org/10.1038/nphys3620.

[94] S. Latini, K. T. Winther, T. Olsen, et al., "Interlayer excitons and band alignment in MoS_2/hBN/WSe_2 van der Waals heterostructures," *Nano Lett.*, vol. 17, pp. 938–945, 2017, https://doi.org/10.1021/acs.nanolett.6b04275.

[95] F. Xia, T. Mueller, Y. Lin, et al., "Ultrafast graphene photodetector," *Nat. Nanotechnol.*, vol. 4, pp. 839–843, 2009, https://doi.org/10.1038/nnano.2009.292.

[96] T. Mueller, F. Xia, and P. Avouris, "Graphene photodetectors for high-speed optical communications," *Nat. Photon.*, vol. 4, pp. 297–301, 2010, https://doi.org/10.1038/nphoton.2010.40.

[97] W. Wang, A. Klots, D. Prasai, et al., "Hot electron-based near-infrared photodetection using bilayer MoS_2," *Nano Lett.*, vol. 15, pp. 7440–7444, 2015, https://doi.org/10.1021/acs.nanolett.5b02866.

[98] Y. Zhang, T. Liu, B. Meng, et al., "Broadband high photoresponse from pure monolayer graphene photodetector, " *Nat. Commun.*, vol. 4, pp. 1811, 2013, https://doi.org/10.1038/ncomms2830.

[99] Q. Guo, A. Pospischil, M. Bhuiyan, et al., "Black phosphorus mid-infrared photodetectors with high gain," *Nano Lett.*, vol. 16, pp. 4648–4655, 2016, https://doi.org/10.1021/acs.nanolett.6b01977.

[100] X. Chen, X. Lu, B. Deng, et al., "Widely tunable black phosphorus mid-infrared photodetector," *Nat. Commun.*, vol. 8, pp. 1672, 2017, https://doi.org/10.1038/s41467-017-01978-3.

[101] D. Schall, D. Neumaier, M. Mohsin, et al., "50 GBit/s photodetectors based on wafer-scale graphene for integrated silicon photonic communication systems," *ACS Photon.*, vol. 1, pp. 781–784, 2014, https://doi.org/10.1021/ph5001605.

[102] D. Schall, C. Porschatis, M. Otto, et al., "Graphene photodetectors with a bandwidth> 76 GHz fabricated in a 6″ wafer process line," *J. Phys. D Appl. Phys.*, vol. 50, pp. 124004, 2017.

[103] R. J. Shiue, Y. Gao, Y. Wang, et al., "High-responsivity graphene–boron nitride photodetector and autocorrelator in a silicon photonic integrated circuit," *Nano Lett.*, vol. 15, pp. 7288–7293, 2015, https://doi.org/10.1021/acs.nanolett.5b02368.

[104] S. Schuler, D. Schall, D. Neumaier, et al., "Controlled generation of a p–n junction in a waveguide integrated graphene photodetector," *Nano Lett.*, vol. 16, pp. 7107–7112, 2016, https://doi.org/10.1021/acs.nanolett.6b03374.

[105] S. Schuler, D. Schall, D. Neumaier, et al., "Graphene photodetector integrated on a photonic crystal defect waveguide, " *ACS Photon.*, vol. 5, pp. 4758–4763, 2018, https://doi.org/10.1021/acsphotonics.8b01128.

[106] P. Ma, Y. Salamin, B. Baeuerle, et al., "Plasmonically enhanced graphene photodetector featuring 100 Gbit/s data reception, high responsivity, and compact size," *ACS Photon.*, vol. 6, pp. 154–161, 2018, https://doi.org/10.1021/acsphotonics.8b01234.

[107] Y. Ding, Z. Cheng, X. Zhu, et al., "Ultra-compact integrated graphene plasmonic photodetector with bandwidth above 110 GHz," *Nanophotonics*, vol. 9, pp. 317–325, 2020, https://doi.org/10.1515/nanoph-2019-0167.

[108] J. Guo, J. Li, C. Liu, et al., "High-performance silicon-graphene hybrid plasmonic waveguide photodetectors beyond 1.55 μm," *Light Sc. Appl.*, vol. 9, pp. 1–11, 2020.

[109] J. E. Muench, A. Ruocco, M. A. Giambra, et al., "Waveguide-integrated, plasmonic enhanced graphene photodetectors," *Nano Lett.*, vol. 19, pp. 7632–7644, 2019, https://doi.org/10.1021/acs.nanolett.9b02238.

[110] J. Sun, E. Timurdogan, A. Yaacobi, et al., "Large-scale nanophotonic phased array," *Nature*, vol. 493, pp. 195–199, 2013, https://doi.org/10.1038/nature11727.

[111] N. Youngblood, C. Chen, S. J. Koester, et al., "Waveguide-integrated black phosphorus photodetector with high responsivity and low dark current," *Nat. Photon*, vol. 9, pp. 247–252, 2015, https://doi.org/10.1038/nphoton.2015.23.

[112] Y. Yin, R. Cao, J. Guo, et al., "High-speed and high-responsivity hybrid silicon/black-phosphorus waveguide photodetectors at 2 μm," *Laser Photon Rev.*, vol. 13, pp. 1900032, 2019.

[113] N. Youngblood and M. Li, "Ultrafast photocurrent measurements of a black phosphorus photodetector," *Appl. Phys. Lett.*, vol. 110, pp. 051102, 2017, https://doi.org/10.1063/1.4975360.

[114] N. Haratipour, Y. Liu, R. J. Wu, et al., "Mobility anisotropy in black phosphorus MOSFETs with HfO_2 gate dielectrics," *IEEE Transact. Electron Devices*, vol. 65, pp. 4093–4101, 2018, https://doi.org/10.1109/TED.2018.2865440.

[115] Y. Liu, T. Low, and P. P. Ruden, "Mobility anisotropy in monolayer black phosphorus due to scattering by charged impurities," *Phys. Rev. B*, vol. 93, pp. 165402, 2016, https://doi.org/10.1103/PhysRevB.93.165402.

[116] R. Soref, "Tutorial: integrated-photonic switching structures," *Apl. Photon.*, vol. 3, pp. 021101, 2018, https://doi.org/10.1063/1.5017968.

[117] J. Song, Q. Fang, S. H. Tao, et al., "Fast and low power Michelson interferometer thermo-optical switch on SOI," *Opt. Express*, vol. 16, pp. 15304–15311, 2008, https://doi.org/10.1364/OE.16.015304.

[118] H. Jayatilleka, K. Murray, M. Á. Guillén-Torres, et al., "Wavelength tuning and stabilization of microring-based filters using silicon in-resonator photoconductive heaters," *Opt. Express*, vol. 23, pp. 25084–25097, 2015, https://doi.org/10.1364/OE.23.025084.

[119] R. Prasher, "Graphene spreads the heat," *Science*, vol. 328, pp. 185–186, 2010, https://doi.org/10.1126/science.1188998.

[120] L. Yu, D. Dai, and S. He, "Graphene-based transparent flexible heat conductor for thermally tuning nanophotonic integrated devices," *Appl. Phys. Lett.*, vol. 105, pp. 251104, 2014, https://doi.org/10.1063/1.4905002.

[121] S. Gan, C. Cheng, Y. Zhan, et al., "A highly efficient thermo-optic microring modulator assisted by graphene," *Nanoscale*, vol. 7, pp. 20249–20255, 2015, https://doi.org/10.1039/C5NR05084G.

[122] D. Schall, M. Mohsin, A. A. Sagade, et al., "Infrared transparent graphene heater for silicon photonic integrated circuits," *Opt. Express*, vol. 24, pp. 7871–7878, 2016, https://doi.org/10.1364/OE.24.007871.

[123] L. Yu, Y. Yin, Y. Shi, et al., "Thermally tunable silicon photonic microdisk resonator with transparent graphene nanoheaters,"

Optica, vol. 3, pp. 159–166, 2016, https://doi.org/10.1364/OPTICA.3.000159.

[124] S. Yan, X. Zhu, L. H. Frandsen, et al., "Slow-light-enhanced energy efficiency for graphene microheaters on silicon photonic crystal waveguides," *Nat. Commun.*, vol. 8, pp. 14411, 2017, https://doi.org/10.1038/ncomms14411.

[125] Z. Xu, C. Qiu, Y. Yang, et al., "Ultra-compact tunable silicon nanobeam cavity with an energy-efficient graphene microheater," *Opt. Express*, vol. 25, pp. 19479–19486, 2017, https://doi.org/10.1364/OE.25.019488.

[126] S. Yu, X. Wu, Y. Wang, et al., "2D materials for optical modulation: challenges and opportunities," *Adv .Mater.*, vol. 29, pp. 1606128, 2017, https://doi.org/10.1002/adma.201606128.

[127] J. M. Dawlaty, S. Shivaraman, J. Strait, et al., "Measurement of the optical absorption spectra of epitaxial graphene from terahertz to visible," *Appl. Phys. Lett.*, vol. 93, pp. 131905, 2008, https://doi.org/10.1063/1.2990753.

[128] B. Sensale-Rodriguez, R. Yan, M. M. Kelly, et al., "Broadband graphene terahertz modulators enabled by intraband transitions," *Nat. Commun.*, vol. 3, pp. 1–7, 2012, https://doi.org/10.1038/ncomms1787.

[129] N. K. Emani, T. F. Chung, X. Ni, et al., "Electrically tunable damping of plasmonic resonances with graphene," *Nano Lett.*, vol. 12, pp. 5202–6, 2012, https://doi.org/10.1021/nl302322t.

[130] Y. Yao, M. A. Kats, P. Genevet, et al., "Broad electrical tuning of graphene-loaded plasmonic antennas," *Nano Lett.*, vol. 13, pp. 1257–64, 2013, https://doi.org/10.1021/nl3047943.

[131] Y. Yao, M. A. Kats, R. Shankar, et al., "Wide wavelength tuning of optical antennas on graphene with nanosecond response time," *Nano Lett.*, vol. 14, pp. 214–219, 2014, https://doi.org/10.1021/nl403751p.

[132] M. M. Jadidi, A. B. Sushkov, R. L. Myers-Ward, et al., "Tunable terahertz hybrid metal–graphene plasmons," *Nano Lett.*, vol. 15, pp. 7099–7104, 2015, https://doi.org/10.1021/acs.nanolett.5b03191.

[133] S. H. Mousavi, I. Kholmanov, K. B. Alici, et al., "Inductive tuning of Fano-resonant metasurfaces using plasmonic response of graphene in the mid-infrared," *Nano Lett.*, vol. 13, pp. 1111–1117, 2013, https://doi.org/10.1021/nl304476b.

[134] S. H. Lee, M. Choi, T. T. Kim, et al., "Switching terahertz waves with gate-controlled active graphene metamaterials," *Nat. Mater.*, vol. 11, pp. 936–941, 2012, https://doi.org/10.1038/nmat3433.

[135] X. Gan, R. J. Shiue, Y. Gao, et al., "High-contrast electrooptic modulation of a photonic crystal nanocavity by electrical gating of graphene," *Nano Lett.*, vol. 13, pp. 691–696, 2013, https://doi.org/10.1364/CLEO_SI.2014.STh1M.1.

[136] B. Sensale-Rodriguez, R. Yan, S. Rafique, et al., "Extraordinary control of terahertz beam reflectance in graphene electro-absorption modulators," *Nano Lett.*, vol. 12, pp. 4518–4522, 2012, https://doi.org/10.1021/nl3016329.

[137] M. L. Brongersma and V. M. Shalaev, "The case for plasmonics," *Science*, vol. 328, pp. 440–441, 2010, https://doi.org/10.1126/science.1186905.

[138] M. Liu, X. Yin, and X. Zhang, "Double-layer graphene optical modulator," *Nano Lett.*, vol. 12, pp. 1482–1485, 2012, https://doi.org/10.1021/nl204202k.

[139] Y. Hu, M. Pantouvaki, J. Van Campenhout, et al., "Broadband 10 Gb/s operation of graphene electro-absorption modulator on

silicon," *Laser Photon Rev.*, vol. 10, pp. 307–316, 2016, https://doi.org/10.1002/lpor.201500250.

[140] H. Dalir, Y. Xia, Y. Wang, et al., "Athermal broadband graphene optical modulator with 35 GHz speed," *ACS Photonics*, vol. 3, pp. 1564–1568, 2016, https://doi.org/10.1021/acsphotonics.6b00398.

[141] C. T. Phare, Y. H. D. Lee, J. Cardenas, et al., "Graphene electro-optic modulator with 30 GHz bandwidth," *Nat. Photon*, vol. 9, pp. 511–514, 2015, https://doi.org/10.1038/nphoton.2015.122.

[142] Y. Ding, X. Zhu, S. Xiao, et al., "Effective electro-optical modulation with high extinction ratio by a graphene–silicon microring resonator," *Nano Lett.*, vol. 15, pp. 4393–4400, 2015, https://doi.org/10.1021/acs.nanolett.5b00630.

[143] Y. Ding, X. Guan, X. Zhu, et al., "Efficient electro-optic modulation in low-loss graphene-plasmonic slot waveguides," *Nanoscale*, vol. 9, pp. 15576–15581, 2017, https://doi.org/10.1039/C7NR05994A.

[144] V. Sorianello, M. Midrio, G. Contestabile, et al., "Graphene–silicon phase modulators with gigahertz bandwidth." *Nat. Photon*, vol. 12, pp. 40–44, 2018, https://doi.org/10.1038/s41566-017-0071-6.

[145] C. Lin, R. Grassi, T. Low, et al., "Multilayer black phosphorus as a versatile mid-infrared electro-optic material," *Nano Lett.*, vol. 16, pp. 1683–1689, 2016, https://doi.org/10.1021/acs.nanolett.5b04594.

[146] R. Peng, K. Khaliji, N. Youngblood, et al., "Midinfrared electro-optic modulation in few-layer black phosphorus," *Nano Lett.*, vol. 17, pp. 6315–6320, 2017, https://doi.org/10.1021/acs.nanolett.7b03050.

[147] R. Peng, C. Chen, and M. Li, *Broadband Waveguide Integrated Black Phosphorus Modulator for mid Infrared Application. CLEO: Science and Innovations*, Optical Society of America, 2018, SM2B.3.

[148] S. Set, H. Yaguchi, Y. Tanaka, et al., "Ultrafast fiber pulsed lasers incorporating carbon nanotubes," *IEEE J. Sel. Top. Quantum Electron*, vol. 10, pp. 137–146, 2004, https://doi.org/10.1109/JSTQE.2003.822912.

[149] V. Scardaci, Z. Sun, F. Wang, et al., "Carbon nanotube polycarbonate composites for ultrafast lasers," *Adv. Mater.*, vol. 20, pp. 4040–4043, 2008, https://doi.org/10.1002/adma.200800935.

[150] F. Wang, A. G. Rozhin, V. Scardaci, et al., "Wideband-tuneable, nanotube mode-locked, fibre laser," *Nat. Nanotechnol.*, vol. 3, pp. 738–742, 2008, https://doi.org/10.1038/nnano.2008.312.

[151] U. Keller, K. J. Weingarten, F. X. Kartner, et al., "Semiconductor saturable absorber mirrors (SESAM's) for femtosecond to nanosecond pulse generation in solid-state lasers," *IEEE J. Sel. Top. Quantum Electron*, vol. 2, pp. 435–453, 1996, https://doi.org/10.1109/2944.571743.

[152] Q. Bao, H. Zhang, Y. Wang, et al., "Atomic-layer graphene as a saturable absorber for ultrafast pulsed lasers," *Adv. Funct. Mater.*, vol. 19, pp. 3077–3083, 2009, https://doi.org/10.1002/adfm.200901007.

[153] Q. Bao, H. Zhang, Z. Ni, et al., "Monolayer graphene as a saturable absorber in a mode-locked laser," *Nano Res.*, vol. 4, pp. 297–307, 2011, https://doi.org/10.1007/s12274-010-0082-9.

[154] J. Sotor, I. Pasternak, A. Krajewska, et al., "Sub-90 fs a stretched-pulse mode-locked fiber laser based on a graphene saturable absorber," *Opt. Express*, vol. 23, pp. 27503–27508, 2015, https://doi.org/10.1364/OE.23.027503.

[155] Y. Cui, F. Lu, and X. Liu., "MoS$_2$-clad microfibre laser delivering conventional, dispersion-managed and dissipative solitons," *Sci. Rep.*, vol. 6, pp. 30524, 2016, https://doi.org/10.1038/srep30524.

[156] M. Zhang, E. J. R. Kelleher, F. Torrisi, et al., "Tm-doped fiber laser mode-locked by graphene-polymer composite," *Opt. Express*, vol. 20, pp. 25077–25084, 2012, https://doi.org/10.1364/OE.20.025077.

[157] Z. Qin, G. Xie, C. Zhao, et al., "Mid-infrared mode-locked pulse generation with multilayer black phosphorus as saturable absorber," *Opt. Lett.*, vol. 41, pp. 56–59, 2016,https://doi.org/10.1364/OL.41.000056.

[158] W. Li, B. Chen, C. Meng, et al., "Ultrafast all-optical graphene modulator," *Nano Lett.*, vol. 14, pp. 955–959, 2014, https://doi.org/10.1021/nl404356t.

[159] Q. Y. Wen, W. Tian, Q. Mao, et al., "Graphene based all-optical spatial terahertz modulator," *Sci. Rep.*, vol. 4, pp. 7409, 2014, https://doi.org/10.1038/srep07409.

[160] P. Weis, J. L. Garcia-Pomar, M. Hoh, et al.,"Spectrally wide-band terahertz wave modulator based on optically tuned graphene," *ACS Nano*, vol. 6, pp. 9118–9124, 2012, https://doi.org/10.1021/nn303392s.

[161] Z. Shi, L. Gan, T.-H. Xiao, et al.,"All-optical modulation of a graphene-cladded silicon photonic crystal cavity," *ACS Photon.*, vol. 2, pp. 1513–1518, 2015, https://doi.org/10.1364/CLEO_AT.2015.JTu5A.73.

[162] L. Yu, J. Zheng, Y. Xu, et al., "Local and nonlocal optically induced transparency effects in graphene–silicon hybrid nanophotonic integrated circuits," *ACS Nano*, vol. 8, pp. 11386–11393, 2014, https://doi.org/10.1021/nn504377m.

[163] M. Ono, M. Hata, M. Tsunekawa, et al., "Ultrafast and energy-efficient all-optical switching with graphene-loaded deep-subwavelength plasmonic waveguides," *Nat. Photon*, vol. 14, pp. 37–43, 2020, https://doi.org/10.1038/s41566-019-0547-7.

[164] H. Chen, S. Nanz, A. Abass, et al., "Enhanced directional emission from monolayer WSe$_2$ integrated onto a multiresonant silicon-based photonic structure," *ACS Photonics*, vol. 4, pp. 3031–3038, 2017, https://doi.org/10.1021/acsphotonics.7b00550.

[165] H. Chen, V. Corboliou, A. S. Solntsev, et al., "Enhanced second-harmonic generation from two-dimensional MoSe$_2$ on a silicon waveguide," *Light Sci. Appl.*, vol. 6, 2017. Art no. e17060, https://doi.org/10.1038/lsa.2017.60.

[166] S. Yang, D. C. Liu, Z. L. Tan, et al., "CMOS-compatible WS$_2$-based all-optical modulator," *ACS Photon.*, vol. 5, pp. 342–346, 2018, https://doi.org/10.1021/acsphotonics.7b01206.

[167] Y. Gao, G. Zhou, H. K. Tsang, et al., "High-speed van der Waals heterostructure tunneling photodiodes integrated on silicon nitride waveguides," *Optica*, vol. 6, pp. 514–517, 2019, https://doi.org/10.1364/OPTICA.6.000514.

[168] D. Popa, Z. Sun, T. Hasan, et al., "Graphene Q-switched, tunable fiber laser," *Appl. Phys. Lett.*, vol. 98, pp. 073106, 2011, https://doi.org/10.1063/1.3552684.

[169] Z. Sun, T. Hasan, F. Torrisi, et al., "Graphene mode-locked ultrafast laser," *ACS Nano*, vol. 4, pp. 803–810, 2010, https://doi.org/10.1021/nn901703e.

[170] Z. Luo, D. Wu, B. Xu, et al., "Two-dimensional material-based saturable absorbers: towards compact visible-wavelength all-fiber pulsed lasers," *Nanoscale*, vol. 8, pp. 1066–1072, 2016, https://doi.org/10.1039/c5nr06981e.

[171] M. Feng, H. Zhan, and Y. Chen, "Nonlinear optical and optical limiting properties of graphene families," *Appl. Phys. Lett.*, vol. 96, pp. 033107, 2010, https://doi.org/10.1063/1.3279148.

[172] H. Liu, Y. Li, Y. S. You, et al., "High-harmonic generation from an atomically thin semiconductor," *Nat. Phys.*, vol. 13, pp. 262–265, 2017, https://doi.org/10.1038/nphys3946.

[173] H. Chen, V. Corboliou, A. S. Solntsev, et al., "Enhanced second-harmonic generation from two-dimensional MoSe$_2$ on a silicon waveguide," *Light Sci. Appl.*, vol. 6, 2017, Art no. e17060, https://doi.org/10.1038/lsa.2017.60.

[174] Y. M. He, G. Clark, J. R. Schaibley, et al., "Single quantum emitters in monolayer semiconductors, " *Nat. Nanotechnol.*, vol. 10, pp. 497–502, 2015, https://doi.org/10.1038/nnano.2015.75.

[175] W. Zhang, C. P. Chuu, J. K. Huang, et al., "Ultrahigh-gain photodetectors based on atomically thin graphene-MoS$_2$ heterostructures," *Sci. Rep.*, vol. 4, pp. 3826, 2014, https://doi.org/10.1038/srep03826.

[176] X. An, F. Liu, Y. J. Jung, et al., "Tunable graphene–silicon heterojunctions for ultrasensitive photodetection," *Nano Lett.*, vol. 13, pp. 909–916, 2013, https://doi.org/10.1021/nl303682j.

[177] C. O. Kim, S. Kim, D. H. Shin, et al., "High photoresponsivity in an all-graphene p–n vertical junction photodetector," *Nat. Commun.*, vol. 5, pp. 1–7, 2014, https://doi.org/10.1038/ncomms4249.

[178] Y. Lee, J. Kwon, E. Hwang, et al., "High-performance perovskite-graphene hybrid photodetector," *Adv. Mater.*, vol. 27, pp. 41–46, 2015, https://doi.org/10.1002/adma.201402271.

[179] X. Guo, W. Wang, H. Nan, et al., "High-performance graphene photodetector using interfacial gating," *Optica*, vol. 3, pp. 1066–1070, 2016, https://doi.org/10.1515/nanoph-2020-0053.

[180] F. Luo, M. Zhu, Y. Tan, et al., "High responsivity graphene photodetectors from visible to near-infrared by photogating effect," *AIP Adv.*, vol. 8, pp. 115106, 2018, https://doi.org/10.1063/1.5054760.

[181] L. Li, W. Liu, A. Gao, et al., "Plasmon excited ultrahot carriers and negative differential photoresponse in a vertical graphene van der Waals heterostructure," *Nano Lett.*, vol. 19, pp. 3295–3304, 2019, https://doi.org/10.1021/acs.nanolett.9b00908.

[182] N. Youngblood, Y. Anugrah, R. Ma, et al., "Multifunctional graphene optical modulator and photodetector integrated on silicon waveguides," *Nano Lett.*, vol. 14, pp. 2741–2746, 2014, https://doi.org/10.1021/nl500712u.

[183] H. Zhou, T. Gu, J. F. McMillan, et al., "Enhanced photoresponsivity in graphene-silicon slow-light photonic crystal waveguides," *Appl. Phys. Lett.*, vol. 108, pp. 111106, 2016, https://doi.org/10.1063/1.4944414.

[184] I. Goykhman, U. Sassi, B. Desiatov, et al., "On-chip integrated, silicon–graphene plasmonic Schottky photodetector with high responsivity and avalanche photogain," *Nano Lett.*, vol. 16, pp. 3005–3013, 2016, https://doi.org/10.1021/acs.nanolett.5b05216.

[185] C. Chen, N. Youngblood, R. Peng, et al., "Three-dimensional integration of black phosphorus photodetector with silicon photonics and nanoplasmonics," *Nano Lett.*, vol. 17, pp. 985–991, 2017, https://doi.org/10.1021/acs.nanolett.6b04332.

[186] Z. Cheng, X. Zhu, M. Galili, et al., "Double-layer graphene on photonic crystal waveguide electro-absorption modulator with 12 GHz bandwidth," *Nanophotonics*, 2019, https://doi.org/10.1515/nanoph-2019-0381.

[187] K. Watanabe, T. Taniguchi, and H. Kanda, "Direct-bandgap properties and evidence for UV lasing of hexagonal boron nitride single crystal," *Nat. Mater.*, vol. 3, pp. 404–409, 2004, https://doi.org/10.1038/nmat1134.

[188] W. Zhang, M. H. Chiu, C. H. Chen, et al., "Role of metal contacts in high-performance phototransistors based on WSe_2 monolayers," *ACS Nano*, vol. 8, pp. 8653–8661, 2014, https://doi.org/10.1021/nn503521c.

[189] Y. Q. Bie, G. Grosso, M. Heuck, et al., "A $MoTe_2$-based light-emitting diode and photodetector for silicon photonic integrated circuits," *Nat. Nanotechnol.*, vol. 12, pp. 1124–1129, 2017, https://doi.org/10.1038/nnano.2017.209.

[190] P. Ma, N. Flöry, Y. Salamin, et al., "Fast $MoTe_2$ waveguide photodetector with high sensitivity at telecommunication wavelengths," *ACS Photon.*, vol. 5, pp. 1846–1852, 2018, https://doi.org/10.1021/acsphotonics.8b00068.

[191] Y. Liu, Y. Huang, and X. Duan, "Van der Waals integration before and beyond two-dimensional materials," *Nature*, vol. 567, pp. 323–333, 2019, https://doi.org/10.1038/s41586-019-1013-x.

[192] N. Flöry, P. Ma, Y. Salamin, et al., "Waveguide-integrated van der Waals heterostructure photodetector at telecom wavelengths with high speed and high responsivity," *Nat. Nanotechnol.*, vol. 15, pp. 118–124, 2020, https://doi.org/10.1038/s41565-019-0602-z.

[193] K. Kang, K. H. Lee, Y. Han, et al., "Layer-by-layer assembly of two-dimensional materials into wafer-scale heterostructures," *Nature*, vol. 550, pp. 229–233, 2017, https://doi.org/10.1038/nature23905.

[194] C. R. Dean, A. F. Young, I. Meric, et al., "Boron nitride substrates for high-quality graphene electronics," *Nat. Nanotechnol.*, vol. 5, pp. 722–726, 2010, https://doi.org/10.1038/nnano.2010.172.

[195] L. Wang, I. Meric, P. Y. Huang, et al., "One-dimensional electrical contact to a two-dimensional material," *Science*, vol. 342, pp. 614–617, 2013.

[196] A. S. Mayorov, R. V. Gorbachev, S. V. Morozov, et al., "Micrometer-scale ballistic transport in encapsulated graphene at room temperature," *Nano Lett.*, vol. 11, pp. 2396–2399, 2011, https://doi.org/10.1021/nl200758b.

[197] F. Withers, O. Del Pozo-Zamudio, A. Mishchenko, et al., "Light-emitting diodes by band-structure engineering in van der Waals heterostructures," *Nat. Mater.*, vol. 14, pp. 301–306, 2015, https://doi.org/10.1038/nmat4205.

[198] R. Soref, "Mid-infrared photonics in silicon and germanium," *Nat. Photon.*, vol. 4, pp. 495–497, 2010, https://10.1038/nphoton.2010.171.

[199] Y. C. Chang, V. Paeder, L. Hvozdara, et al., "Low-loss germanium strip waveguides on silicon for the mid-infrared," *Opt. Lett.*, vol. 37, pp. 2883–2885, 2012, https://doi.org/10.1364/OL.37.002883.

[200] A. Malik, S. Dwivedi, L. Van Landschoot, et al., "Ge-on-Si and Ge-on-SOI thermo-optic phase shifters for the mid-infrared, " *Opt. Express*, vol. 22, pp. 28479–28488, 2014, https://doi.org/10.1364/OE.22.028479.

[201] D. A. B. Miller, D. S. Chemla, T. C. Damen, et al., "Band-edge electroabsorption in quantum well structures: the quantum-confined Stark effect," *Phys. Rev. Lett.*, vol. 53, pp. 2173, 1984, https://doi.org/10.1103/PhysRevLett.53.2173.

[202] D. A. B. Miller, D. S. Chemla, and S. Schmitt-Rink, "Relation between electroabsorption in bulk semiconductors and in quantum wells: the quantum-confined Franz-Keldysh effect," *Phys. Rev. B*, vol. 33, pp. 6976, 1986, https://doi.org/10.1103/physrevb.33.6976.